University of Alberta

The Influence of Sputtering Pressure and Film Thickness on Metal Resistivity

by

Can Xu

A thesis submitted to the Faculty of Graduate Studies and Research
in partial fulfillment of the requirements for the degree of

Master of Science
in
Material Engineering

Department of Chemical and Materials Engineering

Spring 2010
Edmonton, Alberta

Examining Committee

Dr. Kenneth Cadien, Chemical and Materials Engineering

Dr. David Mitlin, Chemical and Materials Engineering

Dr. Douglas Barlage, Electrical and Computer Engineering

ABSTRACT

Electrical resistivity is an important indicator of metal thin film quality. In this study, the influence of argon working pressure on the properties of metal thin films was evaluated, and the thickness effect on the resistivity of metal thin films was investigated. The sputtered thin film resistivity performances of seven metals as a function of argon pressure were measured, and the results turned out that the argon pressure was vital to film quality. Further investigation on sputtered chromium thin films using XRD, SEM and XPS revealed that the argon pressure influences the microstructure of sputtered metal thin films. Different microstructure is the reason for different resistivity performances, and John Thornton's "Zone Model" explains all these behaviours well. The resistivity of aluminum and chromium thin films with thickness from 15 to 150 nm were compared, the resistivity change significantly. The scaling trends are different for different metals.

ACKNOWLEDGEMENTS

I owe my deepest gratitude to my supervisor, Dr. Kenneth Cadien, for his great supervision during my graduate program. This thesis would not have been possible without his incredible patience, outstanding guidance and unreserved help.

My gratitude is also given to Les Schowalter, who kindly trained me to use the tools in the Nanofab. Special thanks to Leslie Cadien for her kindly assistance with reviewing the manuscript.

I sincerely thank Ali Foroughi, Lucy Nolan, Wei Guo and every other member of our research group, from whom I received so much assistance and encouragement.

Finally, I am indebted to my parents in China, for their love, encouragement and support during my whole life.

TABLE OF CONTENTS

LIST OF TABLES

LIST OF FIGURES

LIST OF SYMBOLS

PVD	Physical Vapor Deposition
MEMS	MicroElectroMechanical Systems
VLSI	Very Large Scale Integration
FS	Fuchs-Sondheimer
MS	Mayadas and Shatzkes
DC	Direct Current
BOB	sputtering system #1 in Nanofab facility of University of Alberta
FLOYD	sputtering system #3 in Nanofab facility of University of Alberta
XRD	X-ray diffraction
SEM	Scanning Electron Microscopy
XPS	X-ray Photoelectron Spectroscopy

CHAPTER 1: INTRODUCTION

This research studied two parameters of sputtered metal thin films. The first was the effect of argon working pressure on the resistivity of the films. The second was the size effect of sputtered metal thin films.

Thin film technology has been used widely in industry for years. Sputtering has been one of the most important thin film deposition techniques for a wide variety of commercial and scientific purposes. This study focused on metal thin film sputtering. One of the primary indicators of metal thin film quality is resistivity, and how closely the measured resistivity matches the bulk value for the pure metal [1].

Our group has spent several years in the Nanofab of University of Alberta studying sputtering. It has been observed that various metals deposited by sputter tools with the standard recipes have thin film resistivity values much higher than the bulk metal. This indicates a relatively poor film quality. It is believed that the operating parameter of argon working pressure can greatly affect the microstructure and film properties [2]. The effect of argon pressure during sputtering processing on the resistivity and film quality was evaluated to determine the optimal operating parameter for metal thin film deposition.

As semiconductor fabrication technologies have developed, the scale of

electrical and semiconductor devices has become increasing smaller. When the interconnect dimensions decrease to the order of the mean free path of metal conduction electrons, around 10 to 100nm, the electrical resistivity increases strongly. This size effect has caused problems in the development of smaller microelectronic devices and semiconductor chips [3]. This research was focused on the size effect of metal thin film.

Chapter 2 provides background information about sputtering, the “Zone model” of sputtered metal films and the size effect of metal thin films. Chapter 3 presents the specific experimental procedures used for thin films deposition and thin film characteristic testing methods. Chapter 4 gives the details of the results and discussion of the effect of argon pressure on metal thin film resistivity, as well as the size effect in metal thin films. In chapter 5 conclusions and future work are presented.

CHAPTER 2: LITERATURE REVIEW

2.1 Thin film deposition method sputtering

Sputtering is a widely used Physical Vapor Deposition (PVD) technique. Compared with other kinds of coating techniques, sputtering produces very uniform coatings, and very high deposition rates can be achieved. The deposition temperatures are higher than 300℃ for diode sputtering, and around 100℃ and above for magnetron sputtering. The low temperature of magnetron sputtering enables the use of temperature sensitive substrates [4].

2.1.1 Principle of conventional planar diode sputtering

Sputtering is basically a bombardment and adsorption process. Figure 2.1 schematically represents the principle of conventional diode sputtering [2]. Sputtering processes occur in a vacuum environment. There is a plate of the material to be deposited called the target, and a substrate holder facing the target. The target is connected to a negative voltage supply. A gas, usually argon, is introduced in which a glow discharge can be initialized and maintained.

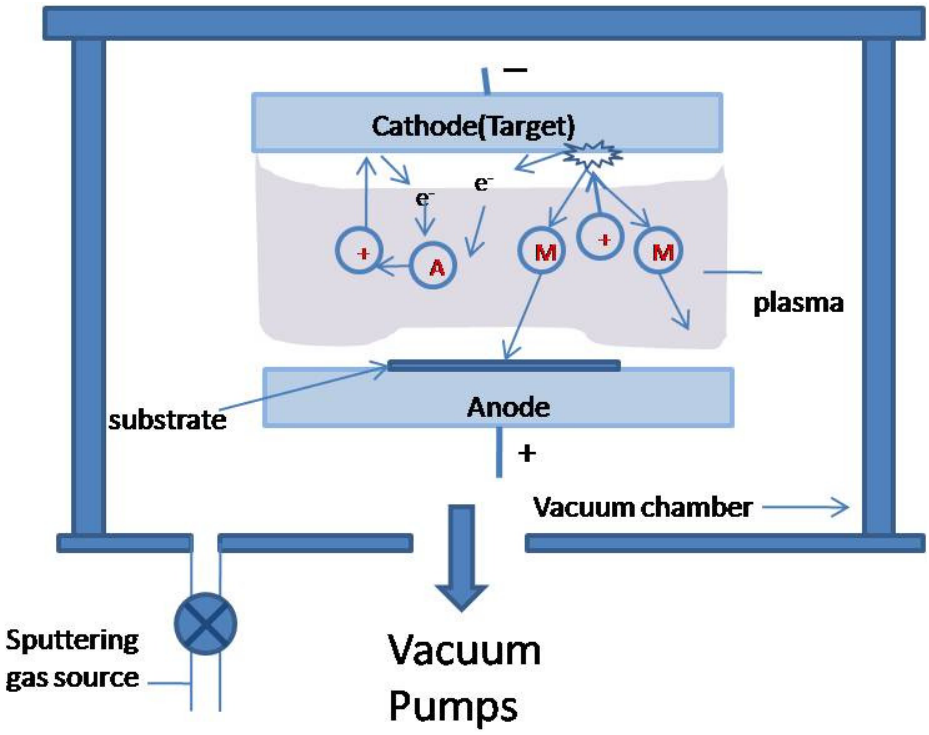

Figure 2.1 A schematic representation of the principle of planar diode sputtering [2]

When a negative voltage is applied to the target, some argon atoms are ionized by free electrons. These positively-charged argon ions are accelerated towards the target and physically bombard the atoms in the target and, through a series of collisions, cause several target atoms to be ejected. Some of the ejected target atoms move towards the substrate and deposit a film on it. During the ion bombardment, in addition to the ejected target atoms, there are other particles and radiation produced such as secondary electrons and ions. The electrons emitted are accelerated by the electrical potential and ionize argon atoms to produce more argon ions.

These electrons, called primary electrons, sustain the discharge. Plasma is produced between the target and the substrate for the sputtering process. Over time, the sputtered target atoms form a continuous thin film on the substrate [2].

The diode sputtering has proven to be a useful technique in the deposition of thin films. However, diode sputtering has problems. As mentioned earlier, primary electrons are important for sustaining the plasma. For diode sputtering, the primary electron mean free path increases with increasing electron energy and decreasing gas pressure. At low argon pressures, the primary electrons travel long distances to collide with argon atoms to produce ions. Therefore, ions are produced far from the cathode and have a greater chance of being lost to the chamber environment (such as walls). Moreover, many primary electrons hit the substrate with high energies, leading to poor film deposition and the loss of primary electrons. Therefore, ionization efficiencies are low and self-sustained discharges cannot be maintained in planar diode sputtering at pressures below about 10 mTorr [5]. Figure 2.2 present a schematic of this phenomenon [2]. On the other hand, at high pressures sputtered atoms have a great probability to be blocked by gas phase collisions with argon atoms [6].

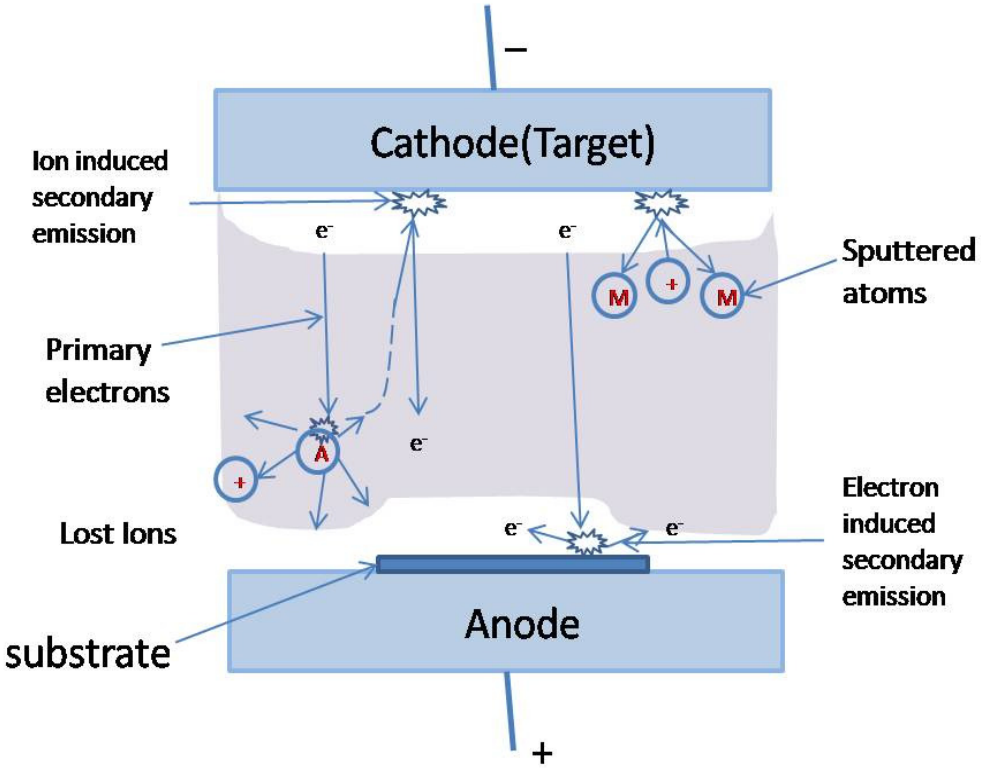

Figure 2.2 A schematic representation of the plasma in planar diode sputtering [2]

2.1.2 Magnetron sputtering

Magnetron sputtering is the most widely used sputtering technique for thin film coating [7]. It has several advantages over diode sputtering. The first advantage of magnetron sputtering is higher deposition rates at equivalent power. Figure 2.3 is a schematic representation of the target in magnetron sputtering [8]. Magnets behind the cathode trap the free electrons in a magnetic field directly above the target surface. These electrons are not free to bombard the substrate to the same extent as in diode sputtering. At

the same time, the extensive, circuitous path carved by these same electrons trapped in the magnetic field, enhances the density of the electrons above the target. This increases the probability of ionizing a neutral gas molecule by several orders of magnitude. This increase in available ions significantly increases the rate at which target material is eroded and subsequently deposited onto the substrate.

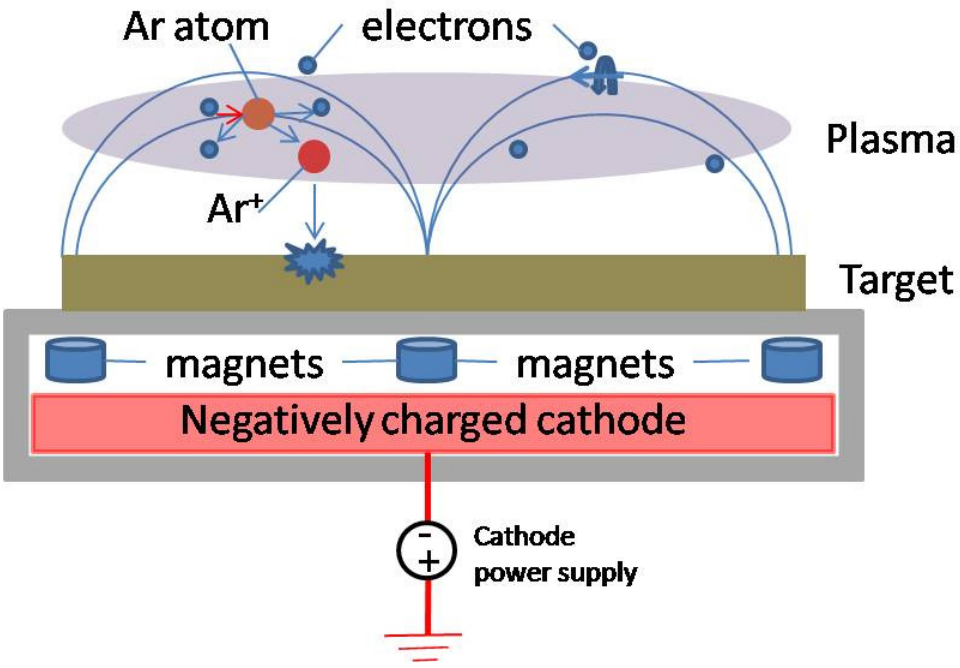

Figure 2.3 A schematic representation of the target in magnetron sputtering [8]

Another important advantage of magnetron sputtering is reduced operating argon pressure. Due to the primary electron trapping and higher ionization efficiency mentioned above, for the same electrode spacing and

minimum target voltage, a stable discharge can be maintained at lower pressures than diode sputtering. Due to lower argon pressure in magnetron sputtering, the sputtered atoms can arrive at the substrate without high probabilities of gas phase collisions and scattering. This improves the efficiency of target atom adhesion and the deposition rate [9].

2.1.3 Reactive sputtering

Reactive sputtering is a sputtering method to deposit certain compound films with metal targets. Compound films such as oxides and nitrides can be deposited in the presence of a reactive gas such as oxygen and nitrogen [10].

2.2 Thin film Properties

Thin film technology has been used in many industries for many years. This has been because thin films can fulfill many specific functions due to their qualities and properties. Generally, there are six categories of thin film properties, namely, optical, electrical, magnetic, chemical, mechanical and thermal [11]. For example, a very thin metal film coating on the back of a sheet of glass can be used to produce two-way mirrors, ferromagnetic thin films for use as computer hard drives [11].

This work focused on electrical properties that play an important role in thin film applications such as MicroElectroMechanical Systems (MEMS) and interconnects in Very Large Scale Integration (VLSI). These

applications are very demanding and benefit from the development of thin film fabrication techniques. The main issue for electronic development is the problem of decreasing dimensions that requires the use of sub 100 nm thick films [3, 12, 13].

This thesis focuses on electrical properties of sputtered metallic thin films. For metallic thin films, one of the most significant properties is the resistivity. A primary indicator of thin metal film quality is how closely the measured film resistivity matches the bulk value for the pure metal [1].

2.3 Influence of operating argon pressure on resistivity and microstructure of sputtered metal thin films

It was reported by J. Thornton and D. Hoffman that resistivity of thin film coatings of many metals such as aluminum, titanium, nickel, molybdenum, tantalum, zirconium, niobium, and tungsten deposited with magnetron sputtering were strongly influenced by the argon pressure [14-16]. Figure 2.4 shows the resistivity of titanium as a function of argon sputtering pressure [15].

Relating different resistivity performance under different argon pressures to the microstructure of thin films, J. A. Thornton developed the “Zone model” in 1974 [17]. Figure 2.5 schematically presents a “Zone model” of metal coating, which describes the influence of argon pressure and substrate temperature on the microstructure of sputtered metallic films.

The diagram was formulated from thick sputtered films (from around 20 to 100 microns) using cylindrical magnetron sputtering [17] [18].

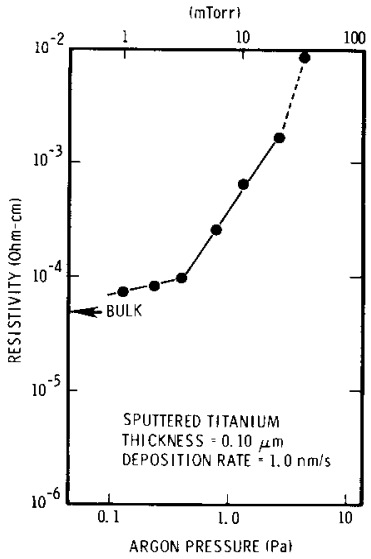

Figure 2.4 Electrical resistivity vs argon working pressure for titanium 100 nm films of given thickness sputtered using magnetron sputtering [15]

As the figure shows, Zone 1 consists of tapered crystallites. Intergrain boundaries of this zone structure are voids rather than true grain boundaries. This leads to a porous structure which has poor lateral strength and low density [17]. Zone T is a transition structure consisting of densely packed but poorly defined fibrous grains. The grains are separated by nearly conventional grain boundaries [17]. Metal coatings with transition structure exhibit high optical reflectance, moderate and relatively low resistivity, and a state of compression [14-16]. Zone 2 structure consists of columnar grains separated by dense intercrystalline boundaries, and Zone 3 consists of recrystallized equiaxed grains [19].

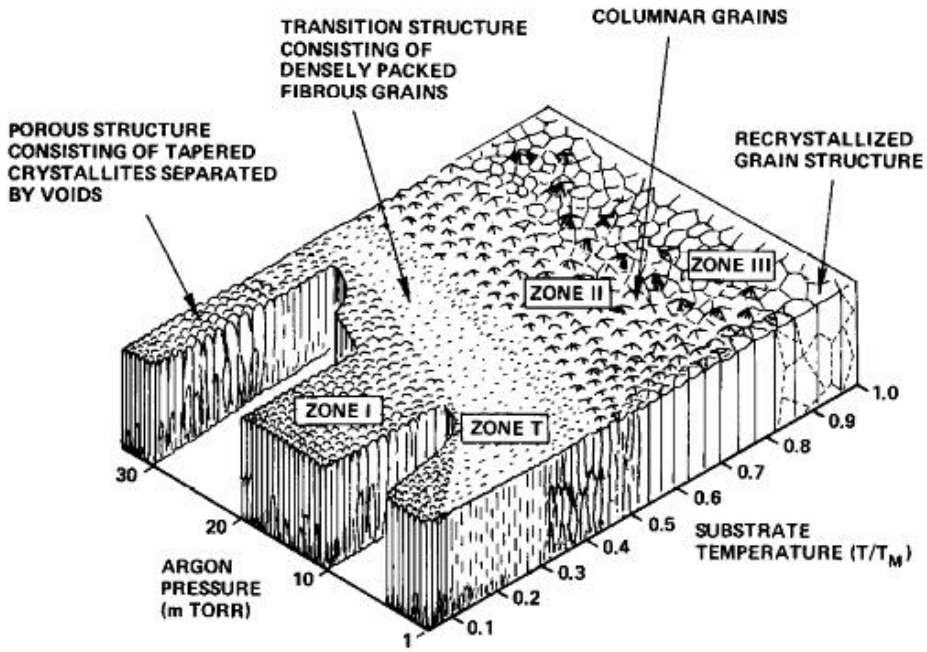

Figure 2.5 “Zone Model” which schematically presents the influence of argon pressure and substrate temperature on microstructure of sputtered metallic films. T is the substrate temperature and Tm is the melting point of the coating material [17] [18]

The mechanism that produces the open Zone 1 structure is not known. However, it is believed to involve a reduction in adatom mobility [17]. In the sputtering process, the inert gas plasma is located between the target and substrate. The pressure of inert gas would affect the mean free path and mobility of adatoms coming from the target and moving to the substrate.

One limitation of Thornton’s “Zone model” is that only inert working gas pressure and substrate temperature are considered for the microstructure of metal coating. Messier et al have further developed the Structure Zone Model by considering the evolution of film morphology and texture as a

function of the substrate voltage bias and film thickness [20]. Barna and Adamik constructed a real structure zone model for polycrystalline metallic films using the effect of impurities in the film as a new deposition parameter responsible for the structure evolution in the films [21].

The Zone model for reactive sputtering has also been developed. Ellmer proposed a complex structure-phase zone model for reactive sputtering of transparent Al-doped ZnO having oxygen partial pressure and the deposition parameters [22].

In this thesis, the effect of argon working pressure on magnetron sputtering of thin metal films at low temperature was studied. Thornton's zone model was used to interpret the results.

2.4 Thickness effect of electrical resistivity of metallic thin films

For a given impurity level, the resistivity of metal films remains constant until the film thickness is less than about 100 nm. This size effect shown in figure 2.6 is a typical diagram of metal film resistivity as a function of film thickness [23]. When the film thickness decreases to the order of the mean free path of conduction electrons, the electrical resistivity of thin metal films increases significantly with further decrease of film thickness. Two additional factors contribute to the total resistivity of thin metal films: surface scattering and grain boundary scattering. This size effect is the subject of active research [24].

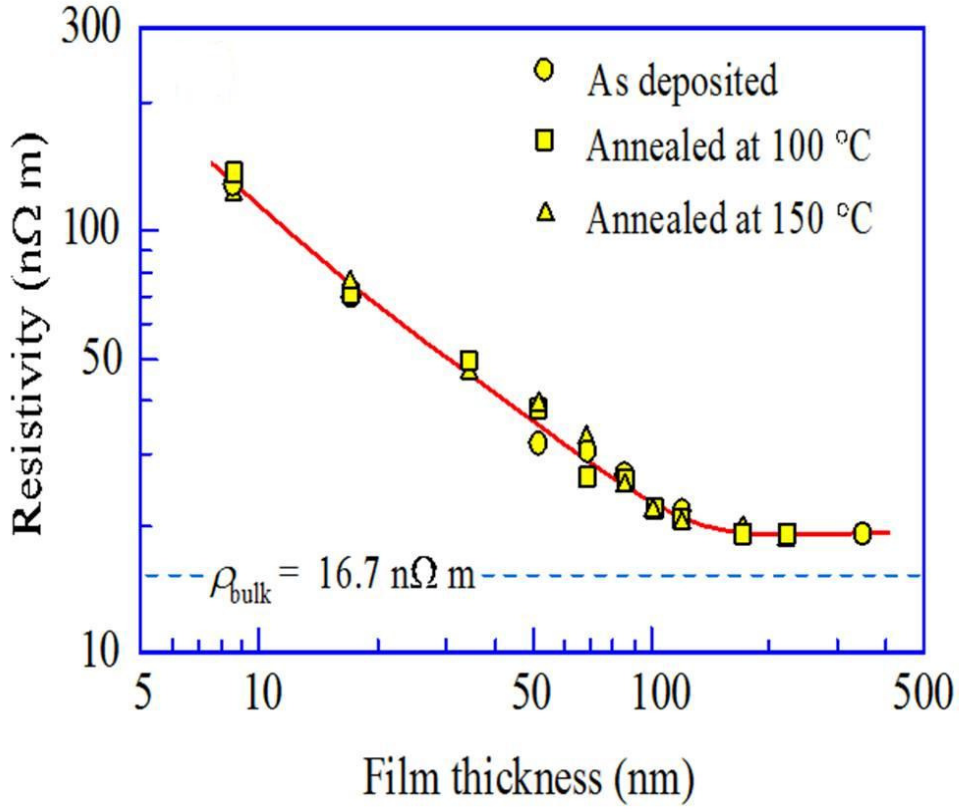

Figure 2.6 Resistivity of Cu films deposited by ion beam deposition as a function of film thickness [23]

The size effect was first attributed to scattering of electrons by the surfaces of the thin films by the Fuchs-Sondheimer (FS) theory [25, 26]. The theory was derived from the Boltzmann transport equations. It introduced a probability p and a ratio k to describe the relationship between film resistivity and surface scattering.

$$\frac{\rho_s(d)}{\rho_0} = [1 - \frac{3}{2k}(1-p)\int_1^{\infty}(\frac{1}{t^3} - \frac{1}{t^5})\frac{1-e^{-kt}}{1-pe^{-kt}}dt]^{-1}$$

Where ρ_s is the film resistivity, ρ_0 is the resistivity of the bulk material, p is

the specular scattering coefficient of the surface and k is the ratio of film thickness (d) to the bulk electron mean free path (λ). The factor p takes values from 0 to 1. For totally elastic scattering (specular reflection), p=0, and for totally inelastic scattering (completely diffuse), p=1.

The influence of grain boundary scattering of thin films was described by another resistivity model, which was also derived from the Boltzmann transport equations, built by Mayadas and Shatzkes in 1970 [27]. Grain boundary scattering is the primary mechanism for the resistivity increase with decreasing thin film thickness in the Mayadas and Shatzkes (MS) theory. The grain boundaries were treated as internal surfaces for calculation in this theory. It introduced two parameters α and R to describe the contribution of grain boundary electron scattering on the resistivity.

$$\frac{\rho_g}{\rho_0} = [1 - \frac{3}{2}\alpha + 3\alpha^2 - 3\alpha^3 \ln(1 + \frac{1}{\alpha})]^{-1}$$

and α is a parameter defined by:

$$\alpha = \frac{\lambda}{d} \cdot \frac{R}{1 - R}$$

Where ρ_g is the resistivity of a polycrystalline thin film, ρ_0 is the resistivity of the bulk material, λ is the mean free path of the electrons for a bulk material, R is the grain boundary reflection coefficient and d is the average grain size of the thin film. The parameter R varies from R = 0 (totally inelastic) up to R = 1 (totally elastic). Typically R is determined from the

equation and experimental data. For example, typical R values of copper are 0.24-0.40 [23]. Figure 2.7 shows simplified models of surface scattering and grain boundary scattering and the appropriate values for P and R.

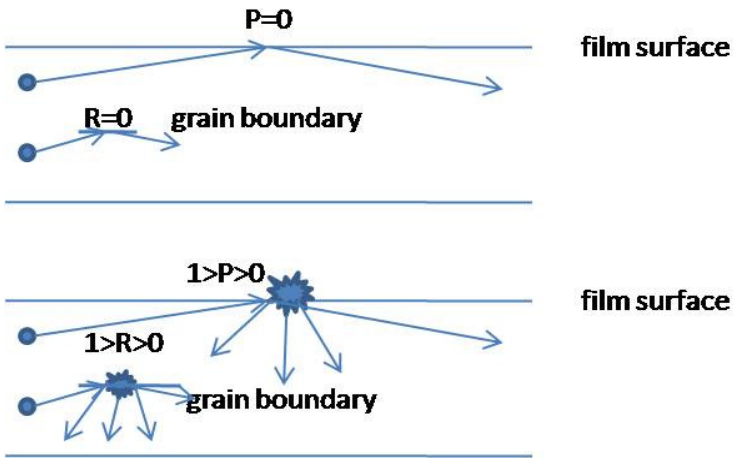

Figure 2.7 Simplified models of surface scattering and grain boundary scattering

Figure 2.8 are AFM scans of 20 nm and 50 nm aluminum films deposited with molecular beam epitaxy at 250℃ which show different grain size with different film thickness [28]. The grain sizes of these two aluminum films are clearly different.

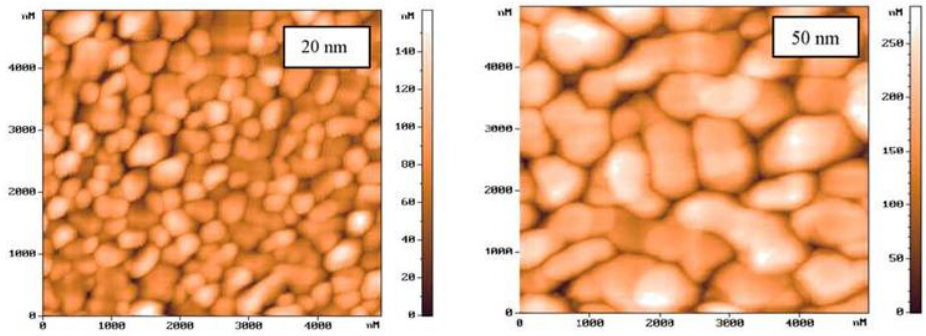

Figure 2.8 AFM scans of 250℃ insitu prepared 20nm and 50nm aluminum films deposited with molecular beam epitaxy [28]

The FS and MS models are two classic theories which have unrealistic assumptions. Numerous studies later focused on fitting thickness effects. There are models built by combining FS and MS models [23, 29, 30]. There are also other models that only work for particular elements [31].

CHAPTER 3: EXPERIMENTAL PROCEDURE

3.1 Introduction

In this work, appropriate metallic thin film sputtering conditions were explored. Also, the resistivity-thickness effect of several kinds of sputtered metallic thin films was studied. Metallic thin films, nano-size in thickness, were deposited onto various substrates under different conditions by a DC magnetron sputtering system. Several thin film properties were measured to evaluate the film quality.

3.2 Substrates and targets

3.2.1 Substrates

Two kinds of substrates were used during this study: microscope glass slides and silicon dioxide/silicon type silicon wafers. The microscope glass slides were 2.54 cm wide × 7.62 cm length, 1.0 mm-1.2 mm in thickness and were manufactured by PEARL Inc. The silicon wafers were 10.16 cm diameter, N-type silicon orientated in (100) direction and were manufactured by Silicon Inc. The thickness of the wafers was approximately 500 μm.

Glass slides are common substrates used for the evaluation of the

sputtering procedure. Glass substrates have little effect on electrical properties of the sputtered thin films. They are transparent insulators with a relatively flat surface. In addition, glass slides are relatively inexpensive. The glass slides were pre-cleaned by an alcohol wash and nitrogen blow dry.

As reviewed earlier in Chapter 2, metal thin films are commonly deposited on silicon dioxide/silicon layers in many kinds of electrical devices. Therefore, silicon dioxide/silicon wafer is another common substrate for sputtered thin film quality tests. The silicon wafers were pre-cleaned in Piranha solution (a mixture of H_2SO_4 and H_2O_2 at volume ratio of 3:1) for 15 minutes. A thermal oxidization process followed; a 200 nm silicon dioxide layer was formed on each wafer. The thermal oxidization process was done in the Minibrute Middle Furnace (Thermal Oxide and General Annealing) in the Nanofab. The process was a 40 minute wet oxidization process at a temperature of 1000℃.

3.2.2. Pure metal targets

Pure metal targets were the sources of the sputtered metal thin films. Seven kinds of metal targets were used. They were aluminum (99.99%), titanium (99.95%), chromium (99.95%), copper (99.99%), zirconium (99.2-99.7% (Grade 702)), niobium (99.95%) and tantalum (99.95%) targets manufactured by Kurt J. Lesker Company. The targets were 7.62cm in diameter, 0.635cm in thickness.

3.3 Thin film deposition

3.3.1 Sputtering process

Sputtering is an important physical vapour deposition (PVD) method for thin film deposition as described earlier. Figure 3.1 illustrates the mechanism of a sputtering process.

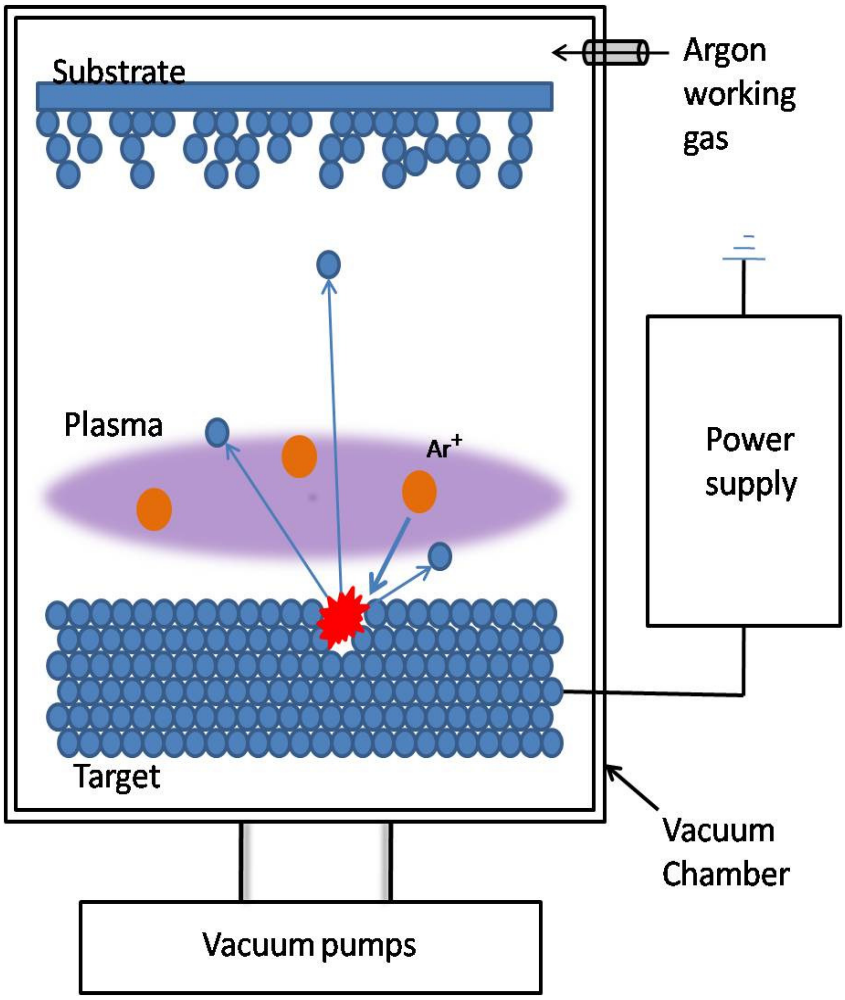

Figure 3.1 Mechanism of sputtering process

Sputtering occurs in an evacuated chamber and is a high vacuum process. A typical sputtering process includes three steps: pumping down the chamber to a high vacuum; backfilling the chamber with argon gas as the working gas; applying power to target and depositing the film. The pump system of a sputtering machine must generate a chamber vacuum pressure lower than 10^{-6} Torr. Vacuum is very important for deposition. The base pressure determines the cleanliness of the chamber and affects the thin film properties. The base pressure used in this work was from 10^{-6} Torr to 10^{-7} Torr. This was achieved with two kinds of pumps: a first stage mechanical pump and a second stage cryopump. The chamber was lowered to 1 mTorr by the mechanical pump. Then the cryopump was used to obtain a vacuum level 10^{-6} Torr to 10^{-7} Torr for sputtering. After evacuation, argon gas was backfilled into the chamber to give a pressure normally from 1 mtorr to 10 mtorr. This is known as the argon working pressure. The argon working pressure is an important factor which will affect the thin film properties. Due to Thornton's “Zone Model”, the substrate temperature and the argon working pressure decide the microstructure of the thin film. The argon pressure also determines the mean free path in the chamber.

3.3.2 Sputtering systems

In this work, metal thin films were deposited in DC planar magnetron sputter systems BOB and FLOYD located in the Nanofab.

As showed in Figure 3.2, Bob is a planar magnetron sputter system with 3 sources in a sputter up configuration. The rotating substrate holder is located at the top of the vacuum chamber. The system has DC power supplies and a lowest base pressure level of 1×10^{-7} Torr. Bob is not capable of heating the substrate [32].

Figure 3.2 Physical Vapor Deposition Magnetron Sputtering System #1 Bob [32]

Figure 3.3 is a schematic diagram of BOB sputtering system. Everything is manual controlled. Sputtering in Bob contains the following steps:

1. Open the chamber and load the substrate and the target. Then close the chamber and pump down the chamber to a base

vacuum level of typically $2.4x10^{-6}$ Torr. The cyropump could get to a vacuum as low as 1×10^{-7} Torr level in the chamber. However, it would take too much time. Normally, the pumping time for Bob is around 1 hour to reach a vacuum level of about 2×10^{-6} Torr.

2. Backfill the chamber with argon gas to the desired pressures. The gate valve also had to be manually adjusted to reach the working pressure.
3. The target holders are tilted towards the substrate holder for possible multi-sources sputtering which wasn't used in this work. The substrate holder rotates during the sputtering for uniformity of the thin film. DC power is applied to the target to start the sputtering process.
4. The target is "cleaned" prior to deposition by striking plasma between the shutter and target.
5. The shutter is opened after 1 minute of sputter cleaning. The thickness of the film was determined by sputter deposition time.

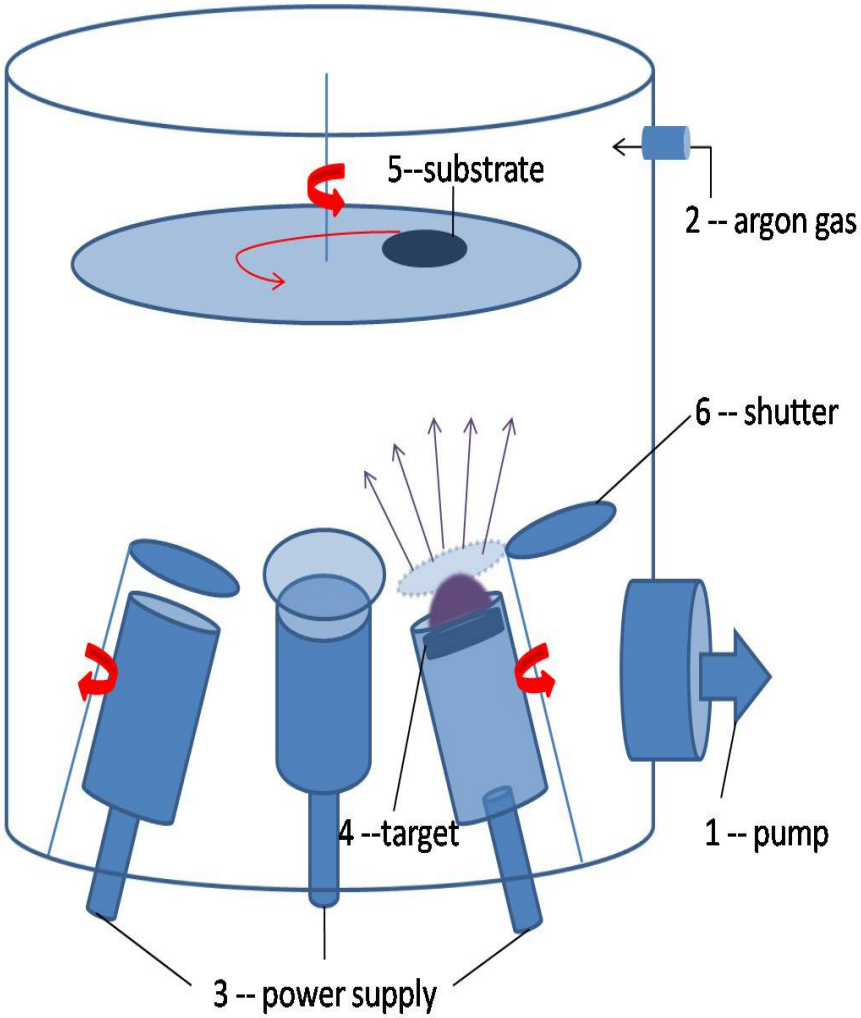

Figure 3.3 A schematic diagram of Bob sputtering system

FLOYD is another planar magnetron sputter system used in this research. FLOYD has four sputter guns and is computer controlled, and load locked. Comparing with BOB, FLOYD has a lower base pressure, cleaner chamber and shorter process time benefit with the load lock system. Most of sputtering steps in FLOYD were automatically controlled with a computer. Argon gas pressure is also controlled with the automatic system. FLOYD has four 7.62 cm planar magnetron sources, which are aluminum,

chromium, gold and titanium nitride sources. Limited sources are a disadvantage of FLOYD. It can easily reach a base pressure level of 1×10^{-7} Torr and has rotating substrate holder [32].

3.4 Experimentation

Two sets of experiments were used to investigate the effects of argon working pressure and film thickness on thin film properties.

3.4.1 Variation of argon working pressure during deposition

The effect of argon working pressure on the resistivity of sputtered metallic thin films was studied. Seven metals were chosen for this investigation as shown in Figure 3.4. They represent metals normally used in thin film technology.

The seven metals were deposited on microscope glass slides using sputtering machine Bob. Depositions were made under the same conditions except different argon pressures were used ranging from 2 to 9 mTorr. The depositions used the same base pressure of $2.4\text{x}10^{-6}$ Torr and same power of 300 W. All film thicknesses were > 120 nm to prevent thickness effects from confounding the resistivity data.

Further investigation of the effect of argon working pressure was made depositing of chromium films with sputtering machine FLOYD. The substrates were 100 mm silicon wafers with a 200 nm silicon dioxide layer.

The base pressure was 3.0 x10^{-7} Torr and the power was 300 W. The argon working pressure range was 1 to 7 mTorr.

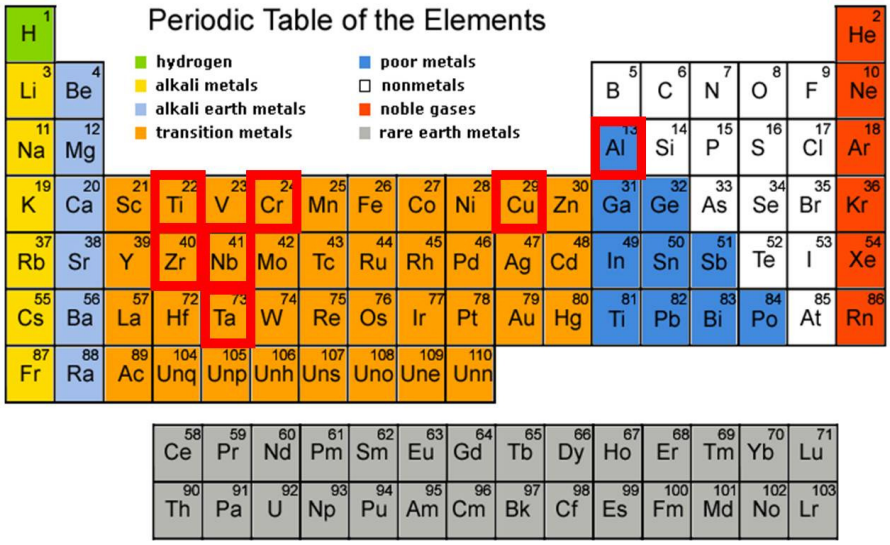

Figure 3.4 The periodic table of the elements. The metals chosen for deposition are shown in red squares [33]

3.4.2 Variation of film thickness

The effect of film thickness, in the low thickness range (less than 150 nm), on the resistivity of metallic thin film was studied. The film thickness was controlled with the deposition time. Aluminum and chromium thin films were deposited with thicknesses varying from 15 to 150 nm using FLOYD. The properties of these thin films were studied to investigate the film thickness effect.

3.4.3 The influence of base pressure

Two different sputtering systems Bob and Floyd were used in this study. The major difference which may affect thin film properties between these two systems was base pressure of the sputtering process. Therefore, with the data from the two sets of experiments, the influence of different base pressures on the resistivity of thin films was studied.

3.5 Thin film Characterization

The following techniques were used to evaluate the properties of the deposited metallic films: four point probe, profilometer, X-ray diffraction (XRD), Scanning Electron Microscopy (SEM), and X-ray Photoelectron Spectroscopy (XPS).

3.5.1 Film resistivity measurement

One of the primary indicators of thin metal film quality is resistivity, and how closely the measured resistivity matches the bulk resistivity for the pure metal. A four point probe was used to measure the sheet resistance of the thin films. Figure 3.5 and Figure 3.6 are photographs of the apparatus and an illustration of the principle of operation of the four point probe, respectively.

Figure 3.5 Four point probe apparatus [32]

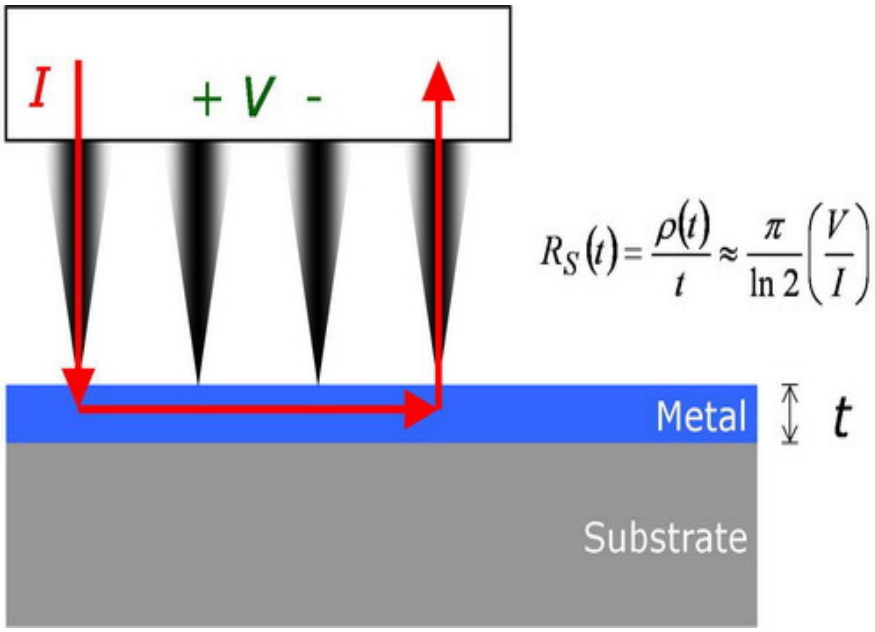

Figure 3.6 The principle of the four point probe

Current *I* is supplied by the two outer probes while the voltage *V* is measured between the two inner probes. Sheet resistance can be directly measured from the device if the probe spacing is known. The resistivity of the film can be calculated with the sheet resistance multiplied by the thickness of the thin film. Equation (3) was derived from equation (1) and (2) and illustrates the relation between film resistivity and sheet resistance.

$$R = \rho * \frac{L}{W * t} \quad (1)$$

$$R = R_s * \frac{L}{W} \quad (2)$$

$$\rho = R_s * t \quad (3)$$

R = resistance (ohm)
R_s = sheet resistance (ohm/cm^2)
ρ = resistivity of the conducting metal film (ohm*cm)
W = Width (cm)
L = Length (cm)
t = Thickness (cm)

Because the sputtered metal thin films are not uniform, normally the sheet resistance values of 8 different sites were measured per sample. The variation of the resistance value of different sites was usually less than 10%, and the average value was used as the sheet resistance for resistivity calculation.

3.5.2 Film thickness measurement

The film thickness was measured with the Alphastep 200 Profilometer in the Nanofab. The Alphastep 200 Profilometer measures the difference in

height (step height) between the substrate and the thin film. Figure 3.7 illustrate the simplified mechanism of the thickness measurement.

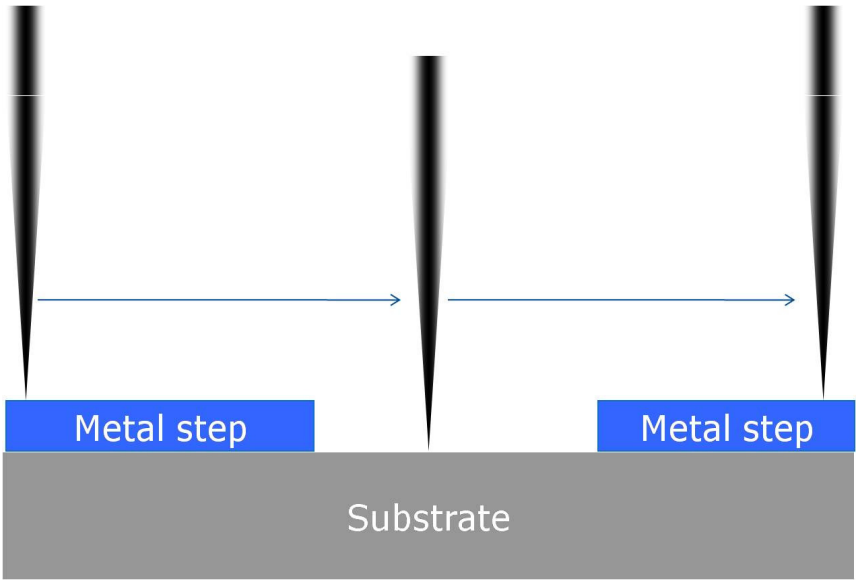

Figure 3.7 Simplified mechanism of the Alphastep 200 Profilometer

A permanent marker was used to draw zig-zag patterns on a cleaned silicon wafer before the deposition. With isopropyl alcohol, the mark can be wiped away after deposition. It gives a clean step for the profilometer to measure the thickness.

Because the sputtered metal thin films are not uniform, the film thicknesses of 4 different sites of the zig-zag pattern were measured per sample. The average value was used as the film thickness.

3.5.3 X-ray Diffraction (XRD)

X-ray diffraction scans were made to investigate the crystallinity of the metallic thin films. XRD scans were made with a wavelength of Cu K_α X-ray source (λ=1.542 Å). The operation conditions were 45 kV, 40 mA. The crystallographic planes of certain thin films would deflect X-rays at particular angles. The crystallinity and crystal plane orientation can be determined with the X-ray diffraction.

XRD analyses of the metal thin films were done by technician Shiraz Merali in the XRD laboratory of the Department of Chemical and Materials Engineering.

3.5.4 Scanning Electron Microscope (SEM)

Scanning Electron Microscopy (SEM) was used to evaluate the film roughness and to depict the morphology of the surface of the thin films at high resolution.

In a SEM, a high-energy beam of electrons is produced at the cathode. The electron beam is accelerated towards the sample and the beam is scanned over the sample surface. The electrons interact with the surface atoms of the sample and produce signals such as secondary electrons and back-scattered electrons. The signals that contain information about the sample's surface properties are captured by a photomultiplier tube and generate the surface SEM images of the samples.

The surface morphology tests in this work were conducted with the SEM which is part of JEOL JAMP-9500F Field Emission Auger Microscope, operated by technician Shihong Xu in the Alberta Centre for Surface Engineering and Science (ACSES).

3.5.5 X-ray photoelectron spectroscopy (XPS)

X-ray photoelectron spectroscopy (XPS) was used to measure the elemental composition of some of the metallic thin films in this work. XPS is a quantitative spectroscopic technique that works under ultra high vacuum (UHV) conditions. XPS spectra are obtained by irradiating a material with a beam of X-rays while measuring the kinetic energy (KE) and number of electrons that escape from the top 1 to 10 nm of the material being analyzed.

The XPS device used in this work was X-ray Imaging Photoelectron Spectrometer Axis Ultra (Kratos Analytical) available at the ACSES facility. XPS analyses of the metal thin films were done by Technician Anquang He.

CHAPTER 4: RESULTS AND DISCUSSION

4.1 The effect of argon working pressure on the resistivity of sputtered metal thin films

Seven kinds of metal were deposited with the sputtering machine BOB. Each metal was deposited under the same conditions except for the argon working pressure. Argon pressures used were between 2 and 9 mTorr.

Tables A1 to A7, found in the Appendix, are the sputtering and resistivity data of the seven sputtered metal thin films. Figures 4.1, 4.2 and 4.3 are based on the experimental data, and show the ratio of resistivity of sputtered metal thin films to their metal bulk resistivity as a function of argon working pressure of the sputtering process. In these figures it can be seen that titanium, chromium, copper, niobium and zirconium films have similar trends. With increasing argon working pressure the resistivity ratio increase significantly. On the other hand, for aluminum and tantalum films, there was little effect of working gas pressure on their resistivity.

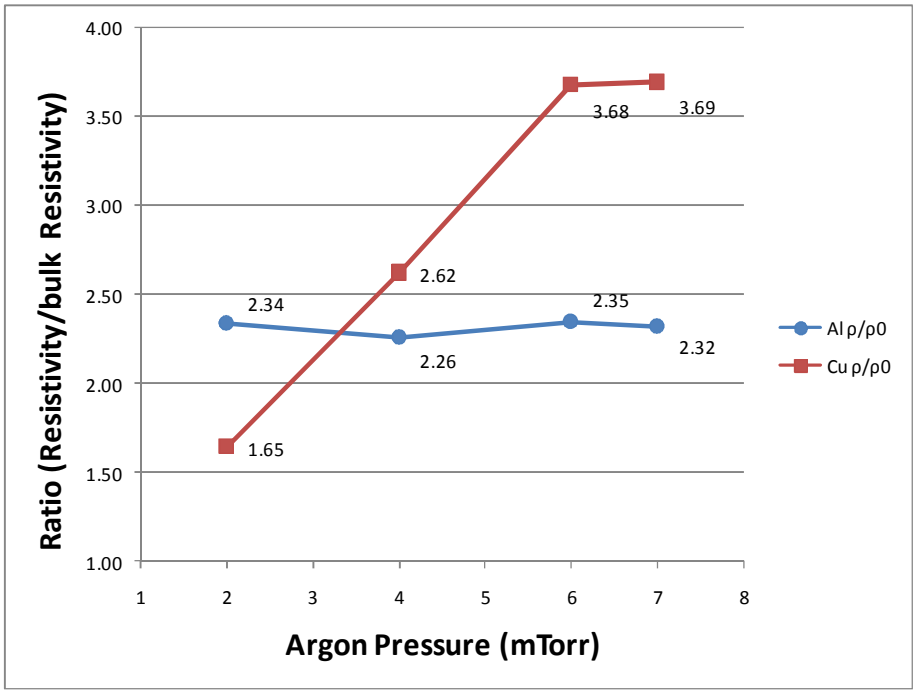

Figure 4.1 The resistivity ratio of film resistivity ratio as a function of argon pressure of metal aluminum and copper

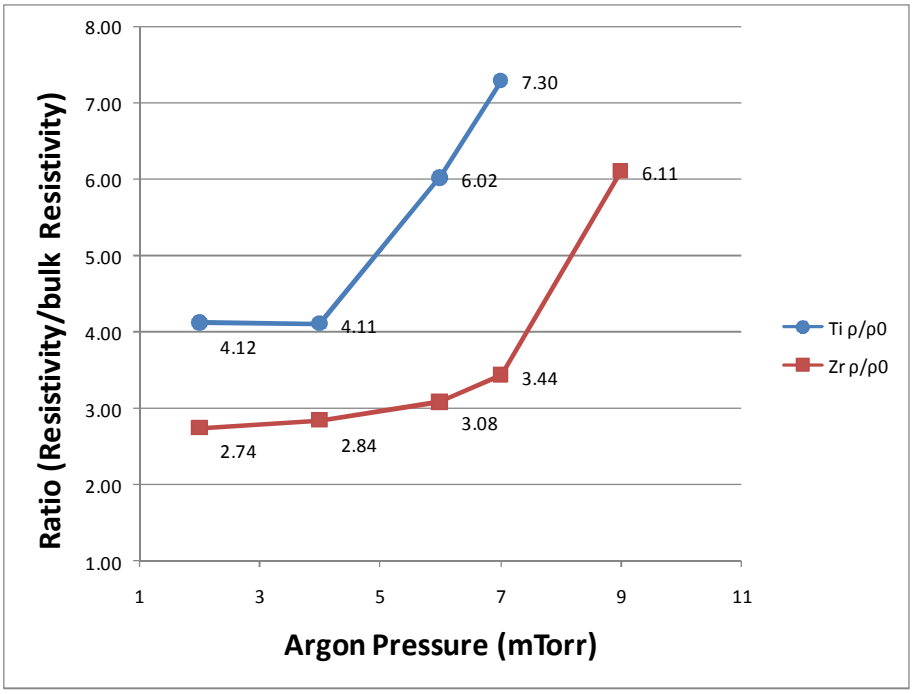

Figure 4.2 The resistivity ratio of film resistivity ratio as a function of argon pressure of metal Titanium and Zirconium.

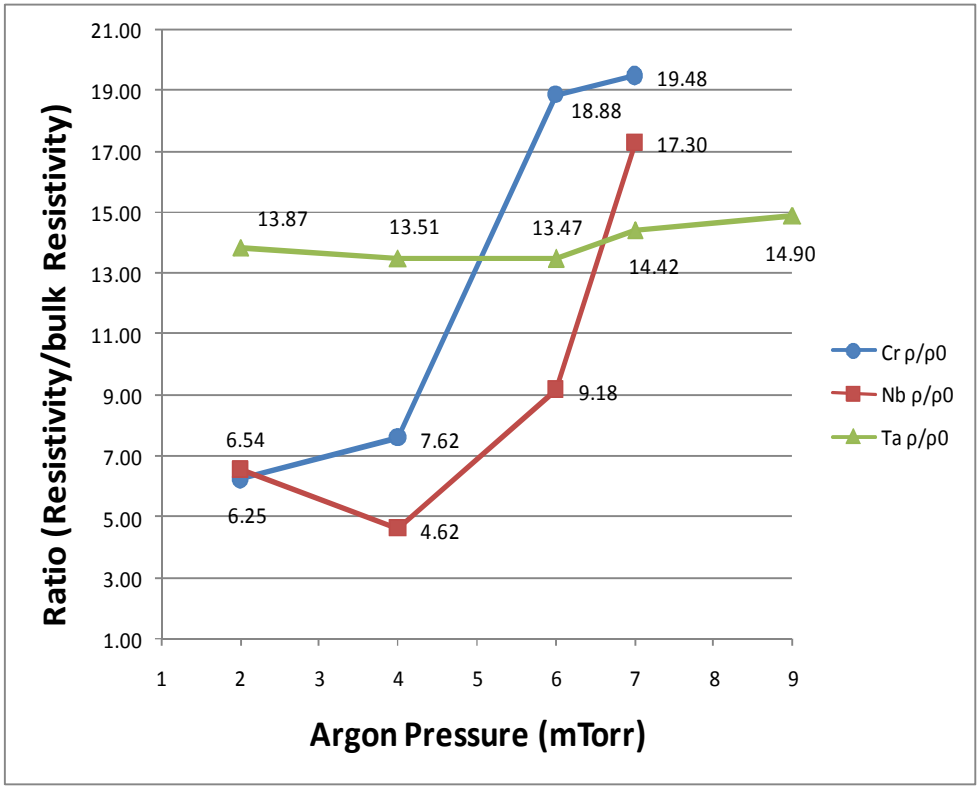

Figure 4.3 The resistivity ratio of sputtered films as a function of argon working pressure of metal chromium, niobium and tantalum.

Table 4.1 shows the maximum and minimum resistivity ratio of the seven metals. The maximum resistivity of the chromium thin film was close to 20 times of that of bulk chromium metal which indicated a poor film quality. Moreover, these five metals show a significant increase of resistivity at certain argon pressure ranges. These ranges are 4 - 7 mTorr for titanium, 2 – 6 mTorr for copper, 4 – 6 mTorr for chromium, 7 - 9 mTorr for zirconium and 4 – 7 mTorr for niobium.

Table 4.1 The ratio of substrate temperature and melting temperature of the seven metals

Metal	$\rho/\rho_{0\,Max}$	Pressure(mTorr)	$\rho/\rho_{0\,Min}$	Pressure(mTorr)
Al	2.35	6	2.26	4
Ti	7.3	7	4.11	4
Cr	19.48	7	6.25	2
Cu	3.69	7	1.65	2
Zr	6.11	9	2.74	2
Nb	17.3	7	4.62	4
Ta	14.9	9	13.47	6

The resistivity ratio of aluminum and tantalum films showed almost no change as argon pressure changed from 2 to 7 mTorr (aluminum) or 2 to 9 mTorr (Tantalum). The aluminum films showed a very low constant value of the ratio (thin aluminum film resistivity and bulk aluminum metal resistivity) which indicated a relatively good thin film quality. On the other hand, tantalum thin films have a very high resistivity compared to the bulk resistivity which indicates relatively poor quality thin films.

Thornton's "Zone Model" [17, 18] suggests that coated thick metal films (around 50 μm in thickness) have great differences in microstructure when sputtered under different argon pressures. It was originally assumed that the Zone Model works on sputtered metal thin films less than 150nm thickness. The microstructures of the thin films would then be decided by the ratio of sputtering temperature to the melting point temperature (T/T_m)

and argon pressure. This relationship is divided into four zones as shown earlier in Figure 2.5. Due to equipment operating conditions, the sputtering experiments were performed at a relatively low substrate temperature of approximately 100℃. For most of the metals used, the homologous temperature, $T/T_{m,}$ is below 0.3. With the argon pressure from 1 – 10 mTorr, the thin films would show microstructure of Zone 1 or Zone T. We expect that metal films with Zone 1 structure will have high resistivity, and those with Zone T will have a much lower resistivity. The T/T_m values of the seven metals in these experiments are listed in table 4.2.

Table 4.2 The ratio of substrate temperature and melting temperature of the seven metals

Metal	Atomic Number	Melting Temperature (K)	Substrate Temperature (K)	T/Tm
Al	13	933	373	0.40
Ti	22	1941	373	0.19
Cr	24	2148	373	0.17
Cu	29	1358	373	0.27
Zr	40	2125	373	0.18
Nb	41	2741	373	0.14
Ta	73	3290	373	0.11

By increasing the argon pressure at small T/T_m, the microstructure changes from Zone T to Zone 1. Zone 1 has a porous structure, consisting of tapered crystallites separated by voids. If exposed to air, the thin film will quickly oxidize leading to poor purity and high resistivity. Zone T, however, has a transition structure of densely packed fibrous grains. The thin films in Zone T would be in compression and have low resistivity.

The experimental data showed that at 150 nm thickness level, the resistivity of low temperature sputtered metal thin films followed the Zone Model. The graphs shown in Figure 4.1, 4.2 and 4.3 showed that an increase of the resistivity ratio occurred in a particular range of argon working pressure which indicated the microstructure change from Zone T to Zone 1.

For the titanium, chromium, copper, zirconium and niobium thin film resistivity ratio curves, there is a flat portion on the graphs below and above key argon pressures. These slight resistivity changes indicate that microstructure of the thin films in these flat regions is not changing.

The resistivity results showed that for many kinds of metals, the argon pressure is an important parameter that affects the film resistivity significantly. For certain metals, sputtering under lower argon pressure results in much better electrical quality of the metal films. However, the variation of the resistivity is not linear. For improved thin film electrical quality, an optimum argon pressure must be evaluated for each metal.

There are two metals, aluminum and tantalum, which showed constant sheet resistivity values in the argon pressure testing. These resistivity results don't conflict with Zone Model. As recorded in Table 4.2, aluminum has a very low melting temperature 660 ℃ and the T/T_m is around 0.4. This T/T_m value is high and the aluminum films remain in Zone T when the argon pressures are varied from 2 to 7 mTorr. This is why the aluminum

film resistivity values are close to bulk value. On the other hand, tantalum has a very high melting temperature of 3017 ℃ and a T/T_m of 0.1. This is low enough to keep the tantalum films in Zone 1 when the argon pressure is varied. This also explains why the resistivity of tantalum films is approximately 14 times the bulk value.

Figure 4.4 shows the predicted extraploted resistivity ratio for aluminum and tantalum over an argon pressure range of < 0.5 to > 10 mTorr. They may have a zone transit which would lead to a significant thin film resistivity change during a higher or lower argon pressure level. However these argon pressures is not obtainable with the Nanofab equipment.

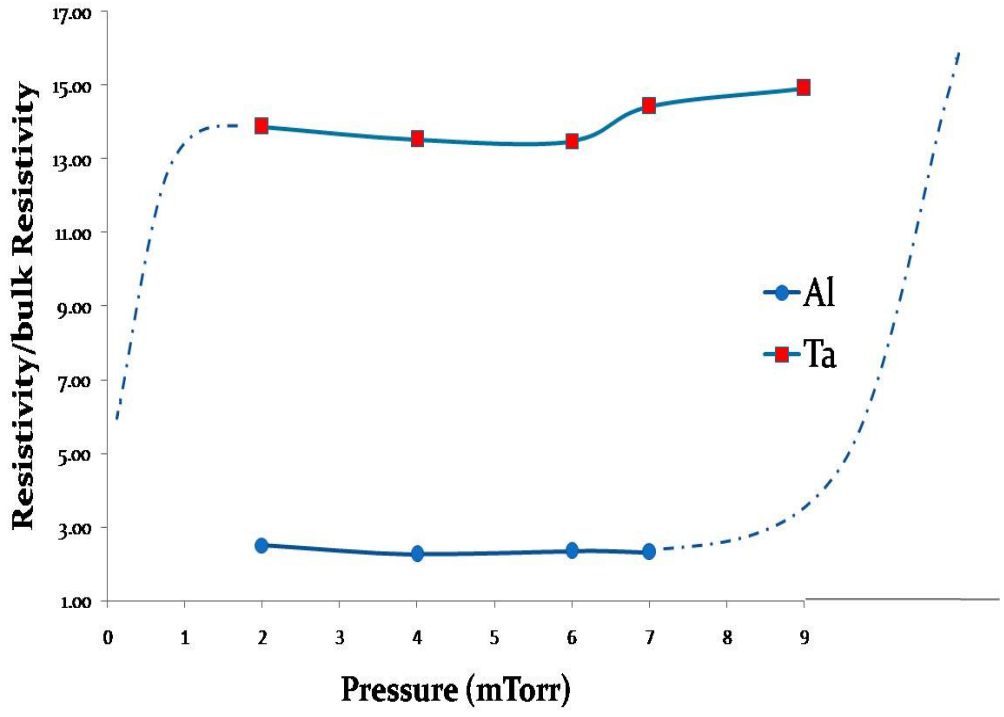

Figure 4.4 The predicted resistivity ratio figure for aluminum and tantalum

4.2 The effect of base pressure on the resistivity of chromium thin film

Chromium showed a typical resistivity ratio change in the testing argon pressure range in the previous experiments. It showed very high resistivity when the argon pressure was above 6 mTorr and a relatively low resistivity when the argon pressure was below 4 mTorr.

Compared to BOB, sputtering machine FLOYD has a lower base pressure and a cleaner environment because it has a load lock. FLOYD can also reach a lower argon pressure of 1 mTorr for chromium. The data for FLOYD-sputtered chromium films is found in table 4.3. The chromium thin films were sputtered on glass substrates, in order to have a direct comparison to films sputtered with Bob.

Figure 4.5 is a plot of the data from table 4.3 and A3 (in Appendix) comparing the chromium resistivity ratios of FLOYD-sputtered films to BOB-sputtered films as argon working pressure is varied. The figure showed that the resistivity ratio curve of FLOYD-sputtered films was lower compared than the BOB-sputtered films resistivity ratio curve. The variation trend of resistivity ratio was similar, but the resistivity ratios were clearly lower under the same argon pressure.

Table 4.3 Sputtering data of chromium thin film sputtered with Floyd

P(mTorr)	1	2	4	6	7	Pressure
Rs(Ω/m2)	1.699	2.179	5.490	10.863	11.796	Average sheet resistance
t(nm)	151.5	152.5	150	155	147.5	Average thickness
ρ(Ω·m)	2.57E-07	3.32E-07	8.24E-07	1.68E-06	1.74E-06	Resistivity
ρ_0(Ω·m)	1.25E-07	1.25E-07	1.25E-07	1.25E-07	1.25E-07	Bulk resistivity
ρ/ρ_0	2.06	2.66	6.59	13.47	13.92	Ratio

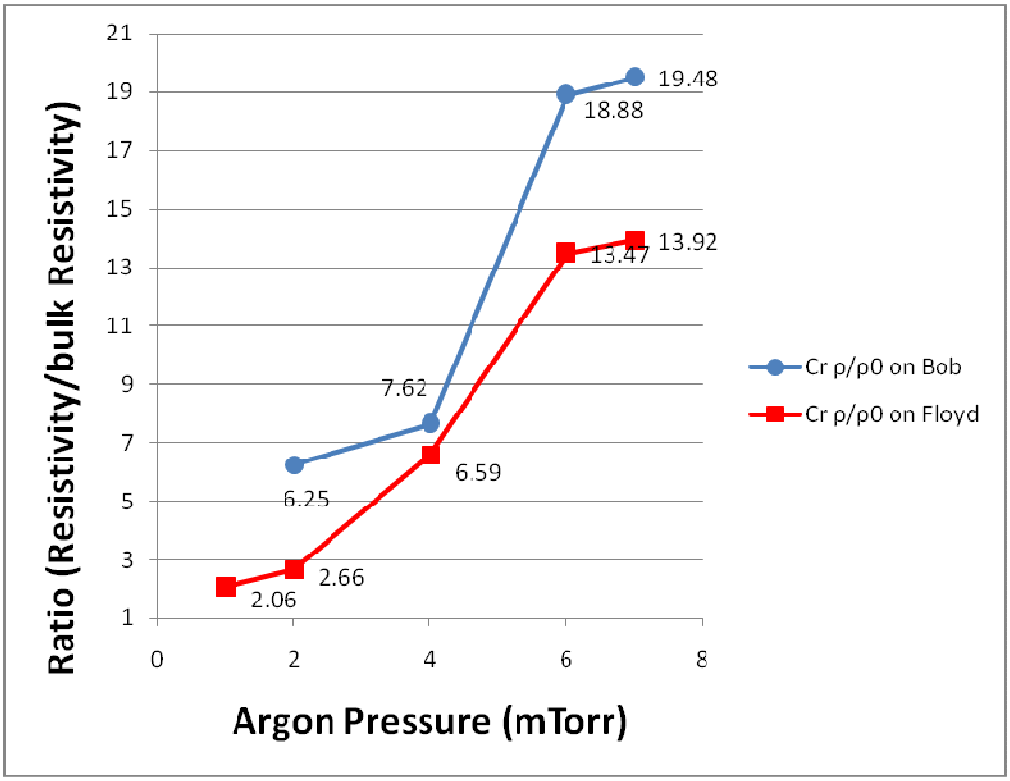

Figure 4.5 The chromium resistivity ratios on Bob and Floyd as a function of argon pressure

The major difference between the FLOYD and BOB systems is the “cleanliness” of the chamber during the sputtering. This comes from two factors. Firstly, the base pressure of FLOYD is approximately 10 times lower than that of BOB. Typically FLOYD has a base pressure of around 3.0×10^{-7} Torr and we used 2.4×10^{-6} Torr as the base pressure of Bob. Therefore, the difference in base pressure means the difference pressure of residual air in the chamber. The residual air, particularly the oxygen content of air, can oxidize the metal thin film during the sputtering process. The electrical resistivity of metallic oxides is much higher than pure metals, and the metallic oxide component would affect the resistivity of the metallic thin film. The second factor is that FLOYD has a load lock system. The samples are placed in the sputtering chamber through the load lock system without opening the chamber itself. It allows the sputtering chamber to be under vacuum at all times. Therefore, with a load lock system, there are barely air molecules adsorbed by the chamber wall and the virtual leak effect of the vacuum system is minimized.

The comparison of resistivity of chromium thin films sputtered with FLOYD and BOB systems showed that the base pressure and cleanliness of the chamber are important issues affecting the film quality. Sputtering systems with lower base pressure and load lock systems can produce metal thin films with better electrical quality.

4.3 The influence of argon working pressure on the microstructure of chromium thin films

In order to further investigate the film qualities and prove that the Zone Model applies to the nanoscale, it was decided to further investigate the structure of the films using X-ray diffraction, SEM, XPS. All of the tests used chromium thin films sputtered with sputtering machine FLOYD. The thin films were sputtered on 100 mm silicon wafers with 200 nm thick silicon dioxide layer. The thicknesses of the chromium thin films were around 150 nm as measured with the profilometer. They were sputtered at argon pressure ranging from 1 to 7 mTorr.

X-ray diffraction tests were used to reveal the crystallinity of the chromium thin films. Table 4.4 shows the X-ray diffraction peaks of the chromium thin film sputtered under 1 mTorr, 4 mTorr and 7 mTorr argon pressure compared to powder chromium peaks from the X-ray database. It was seen that the X-ray diffraction peaks basically exhibit similar characteristics, matching the peaks of chromium powders. The main four peaks of the patterns matched four peaks of one powder chromium diffraction data in the testing 2θ range from the database. The X-ray diffraction patterns showed that the chromium films have polycrystalline microstructure and (110) preferred orientation.

Table 4.4 XRD peaks recorded for chromium films sputtered under different argon pressure 1 mTorr, 4 mTorr and 7 mTorr compared to certain chromium powder peaks

Intensity / Different Sample	I(110)	I(200)	I(211)	I(220)
7 mTorr	100.0	10.9	15.7	5.3
4 mTorr	100.0	12.5	13.2	3.8
1mTorr	100.0	11.7	10.8	2.7
Powder	100.0	15.8	29.8	9.0

To have visual images of the microstructures of the thin films, SEM was used. Several SEM images at 50,000x and 100,000x were captured to differentiate the surface microstructure of the chromium films sputtered under different argon pressures. Figure 4.6 reveals that the surface microstructures of chromium thin film sputtered under 1 mTorr and 7 mTorr are significantly different. The chromium film sputtered at 1 mTorr presents a smooth and dense surface compared to 7 mTorr sputtered chromium film. The structure exhibited poorly defined fibrous grains without clear boundaries. The chromium film sputtered under 7 mTorr, however, showed a rougher surface and possible evidence of porosity. The film surface consisted of small crystallites separated by voids. The crystallites were poorly bonded to each other because of the voids. The images of the films

fit the Zone Model. The microstructure of chromium film sputtered under 1 mTorr indicates the transition structure of Zone T, and the 7 mTorr film exhibited the porous characteristics of Zone 1.

SEM images in Figure 4.7 show microstructure changes in chromium films grown under sputtering pressure from 1 mTorr to 7 mTorr. The microstructure first presents poorly defined grains at 1 mTorr. No clear boundaries, no significant depths change. As the argon pressure increase to 2 mTorr, the crystallites and clear boundaries of grains start to appear. In 3 mTorr image, these grains occupied the whole area. As the argon pressure further increases to 4 mTorr, voids between the crystallites start to appear. Note that in the resistivity diagram, 4 mTorr is the first data point with remarkable resistivity increase. This may indicate that these voids are the most possible reason of the significant variation of film resistivity. From the 6 mTorr and 7 mTorr images, the films are appear to be full of voids and the crystallites are completely separated by these voids, which also correspond with the high film resistivity.

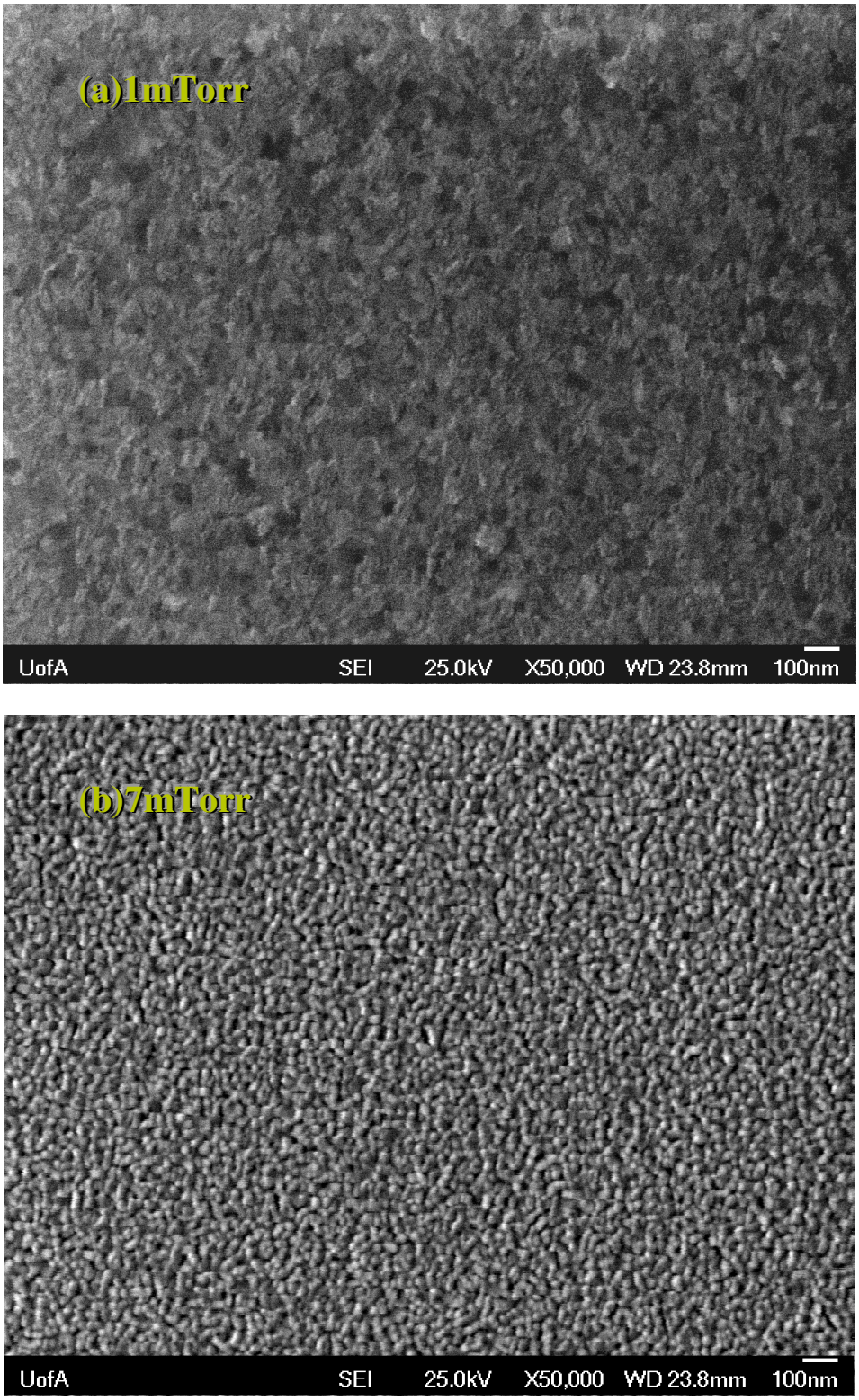

Figure 4.6 SEM images of surface of chromium thin films sputtered under different argon pressure at 50,000x: (a) 1 mTorr (b) 7 mTorr

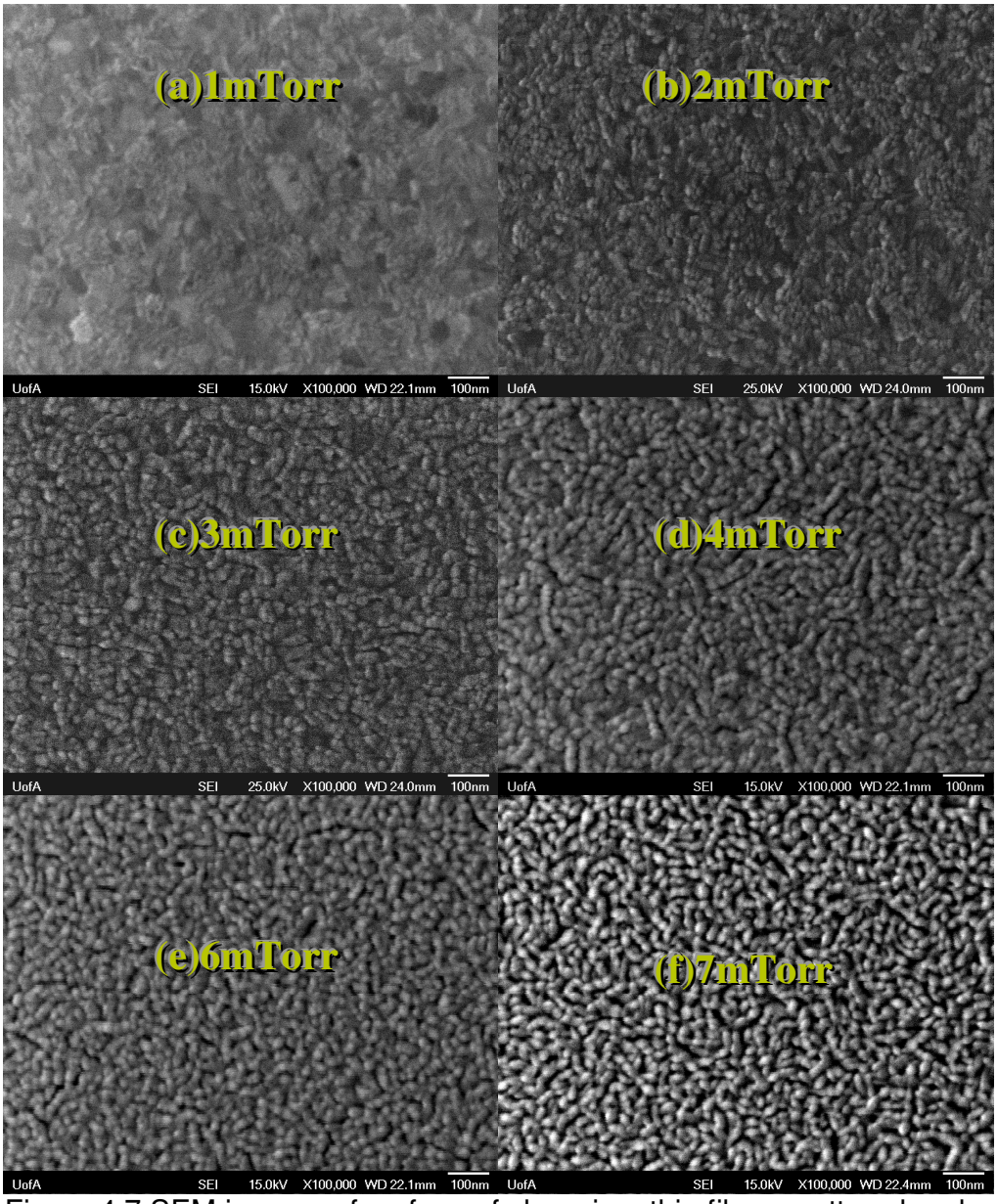

Figure 4.7 SEM images of surface of chromium thin films sputtered under different argon pressure at magnification factor 100,000x: (a) 1 mTorr (b) 2 mTorr (c) 3 mTorr (d) 4 mTorr (5) 6 mTorr (6) 7 mTorr

The composition of the surface of the chromium films sputtered at 1 mTorr and 7 mTorr argon pressure were measured using XPS. Prior to testing, physical sputter etching was done to remove the surface layer which was oxidized due to exposure to air. From the data from the ACSES facility, the etching speed was around 5 nm/min. Etching times of 1 and 4 minutes produced chromium film samples that had 5 and 20 nm removed, respectively.

Figure 4.8 is a full map XPS spectra of binding energy of chromium film sputtered under 7 mTorr with 1 minute etching. From the peaks in the full map XPS spectra identified by software, composition of elements can be calculated. The main shape of full map of XPS spectra of chromium film sputtered under 1 mTorr is similar to figure 4.8.

Table 4.5 is the calculated compositions of the 2 samples. The purity of the chromium film sputtered under 1 mTorr is much better than the film sputtered under 7 mTorr. The 1 mTorr film contains much less oxygen component than 7 mTorr film. Porous structure of the 7 mTorr thin film sample and densely compact structure of the 1 mTorr thin film should be the reason of the composition differences. The porous structure lead to lower purity naturally and also provides much larger contact area for oxidation.

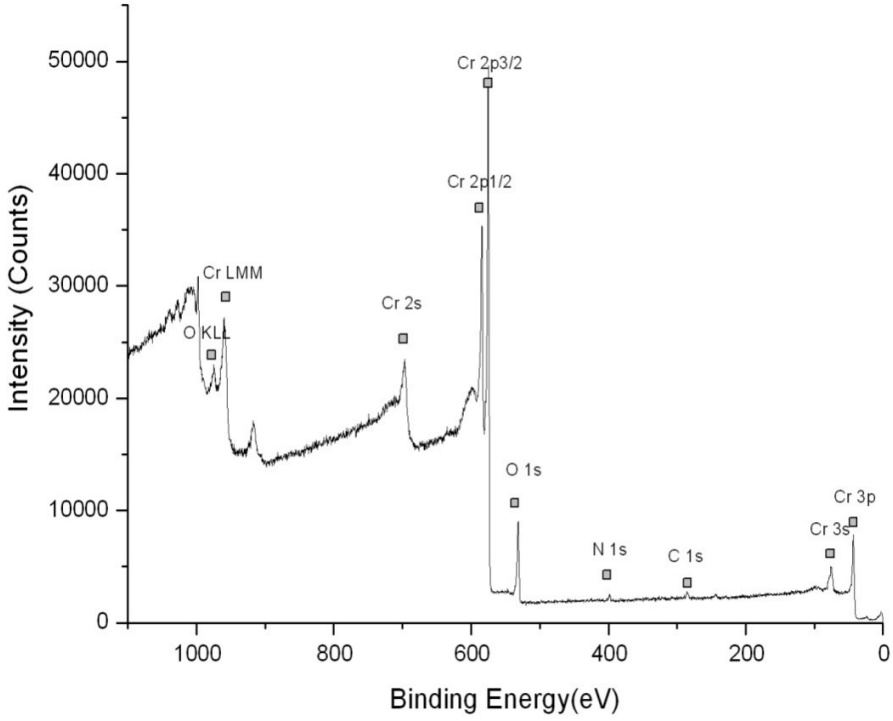

Figure 4.8 XPS patterns of sputtered chromium thin film

Table 4.5 Surface composition of chromium films measured with XPS

Sample #1 Chromium thin film sputtered under argon pressure 1 mTorr

Physical etch 1min	Atomic Conc.%	Mass Conc.%		Physical etch 4min	Atomic Conc.%	Mass Conc.%
Cr 2p	89.11	96.62		Cr 2p	89.76	96.96
O 1s	7.19	2.4		O 1s	5.54	1.84
N 1s	1.25	0.37		N 1s	0.73	0.21
C 1s	2.45	0.61		C 1s	3.97	0.99

Sample #2 Chromium thin film sputtered under argon pressure 7 mTorr

Physical etch 1min	Atomic Conc.%	Mass Conc.%		Physical etch 4min	Atomic Conc.%	Mass Conc.%
Cr 2p	66	87.1		Cr 2p	79.22	93.06
O 1s	23.66	9.61		O 1s	13.76	4.97
N 1s	2.81	1		N 1s	1.4	0.44
C 1s	7.53	2.3		C 1s	5.62	1.53

More importantly, with further physical sputter etching, the chromium composition in 1 mTorr film showed little change. However, the composition of chromium in 7 mTorr film increased around 13%. This was considered more evidence of the Zone 1 and Zone T structures of chromium films sputtered under different argon pressures. The steady composition of chromium in 1 mTorr film was evidence of compact transition structure of Zone T. The tapered structure of the 7 mTorr chromium film leads to increased oxygen content approaching to the surface of the thin film.

Figure 4.9 shows the Cr_{2p} core level XPS spectra of 150 nm chromium thin film deposited at 7 mTorr argon pressure. The Cr_{2p} core level XPS spectra contain two peaks which are $Cr_{2p1/2}$ and $Cr_{2p3/2}$ core level peaks. As the figure shows, the peaks are unbalanced. To analyze the bond type of chromium of the thin film, CasaXPS analysis software (licensed by ACSES) was used to analyze the $Cr_{2p3/2}$ peak of chromium thin film. As Figure 4.10 shows, the $Cr_{2p3/2}$ core level peak consisted of two component peaks. One of them is located at around binding energy 574.5 eV which indicates a Cr-Cr bond. The other, located at around binding energy 575.9 eV, indicates a Cr-O bond of Cr_2O_3. The Cr-O binding energy level is around 1eV higher than Cr-Cr binding energy level. The figure proves the existence of the chromium oxidation.

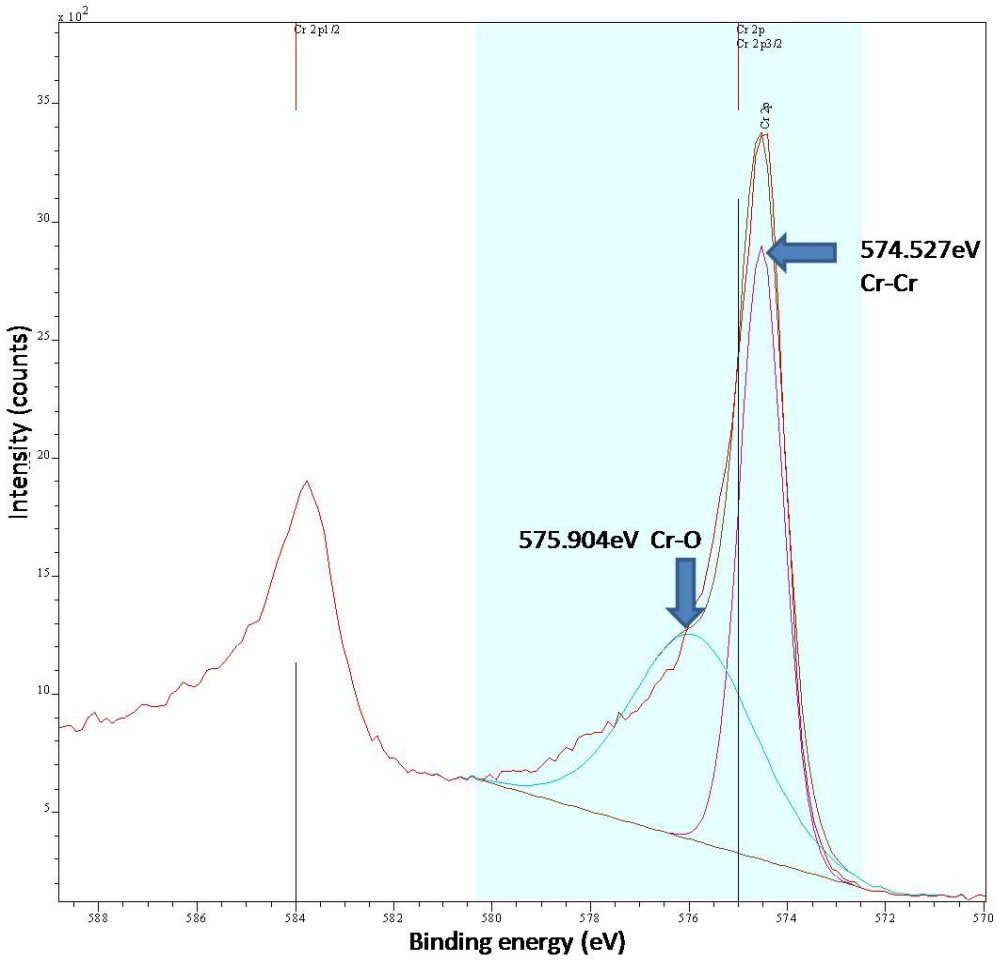

Figure 4.9 High resolution XPS spectra of Cr 2p core level of the sputtered chromium thin film deposited at 7 mTorr argon pressure

Figure 4.10 shows the high resolution XPS spectra of $Cr_{2p3/2}$ core level of the sputtered chromium thin film deposited at different argon pressure 1 mTorr and 7 mTorr. As indicated by arrows, the relative height of the shoulder of the peak of the 7 mTorr chromium thin film is higher than the 1 mtorr chromium film. The shoulder of the peaks should be compared

using relative height of its main peak. Recalling the peak analysis in Figure 4.9, the shoulder located in the higher binding energy side indicates the component of Cr-O bond. Therefore, the chromium thin film sputtered under 7 mTorr argon pressures contains more chromium oxide. This is possible evidence of porous structure of chromium thin film sputtered under 7 mTorr.

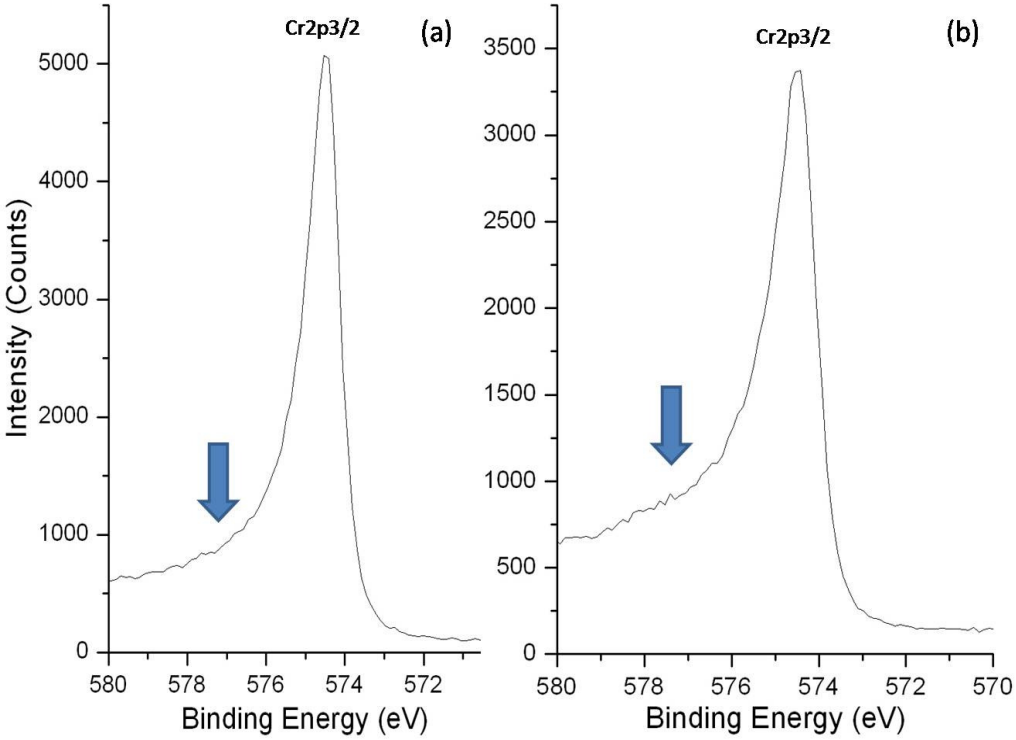

Figure 4.10 High resolution XPS spectra of $Cr_{2p3/2}$ core level of the sputtered chromium thin film deposited at: (a) 1 mTorr argon pressure, (b) 7 mTorr argon pressure.

4.4 The effect of film thickness on the properties of aluminum and chromium thin films

To determine the effect of film thickness on electrical properties, aluminum and chromium thin films with thickness from 15 nm to 150 nm were sputtered in the FLOYD system. The films were sputtered on silicon wafers with a 200 nm silicon dioxide layer.

Figure 4.11 shows the variation of the resistivity of sputtered aluminum and chromium thin films as a function of film thickness. The curves showed a similar shape for the two elements. The resistivity of the films is influenced by film thickness. The resistivity of the resistivity increased when the film thickness decreased and this variation is much stronger when the thicknesses are less than 60 nm. Experimental data is found in the Appendix Table A8 and A9.

Figure 4.12 shows that as the film thickness decreased, the resistivity ratio changes of the metals are different. With decreasing film thickness, the resistivity ratio (film resistivity / bulk metal resistivity) of aluminum thin films had a stronger increasing trend than the resistivity ratio of chromium thin films. Note that the resistivity value of chromium is higher than aluminum as shown in figure 4.11.

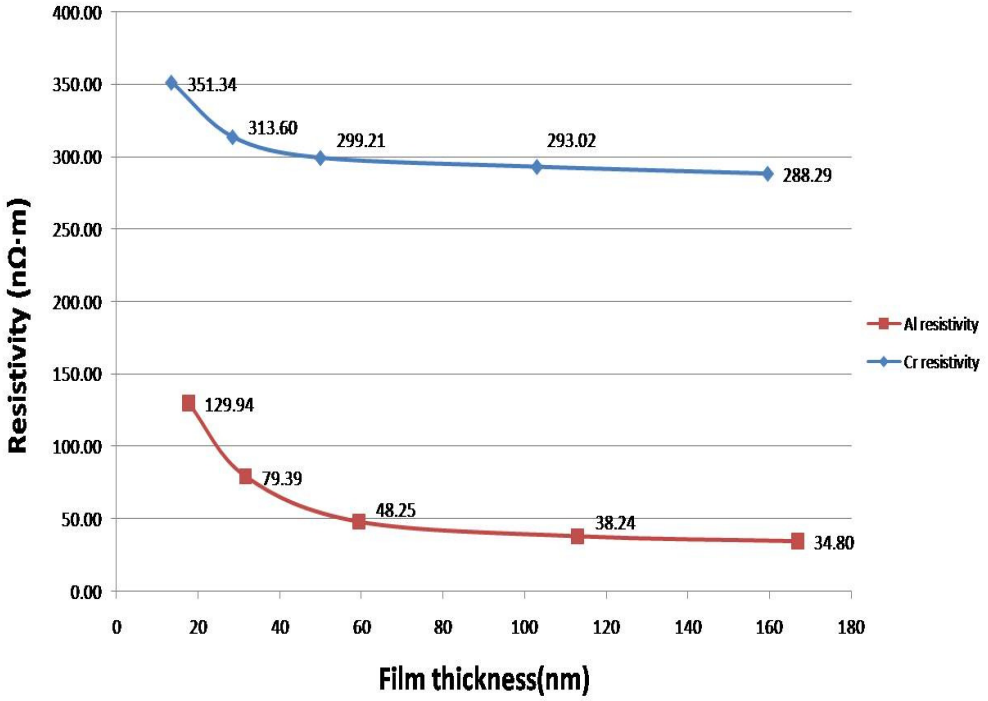

Figure 4.11 The aluminum and chromium resistivity values as a function of film thickness

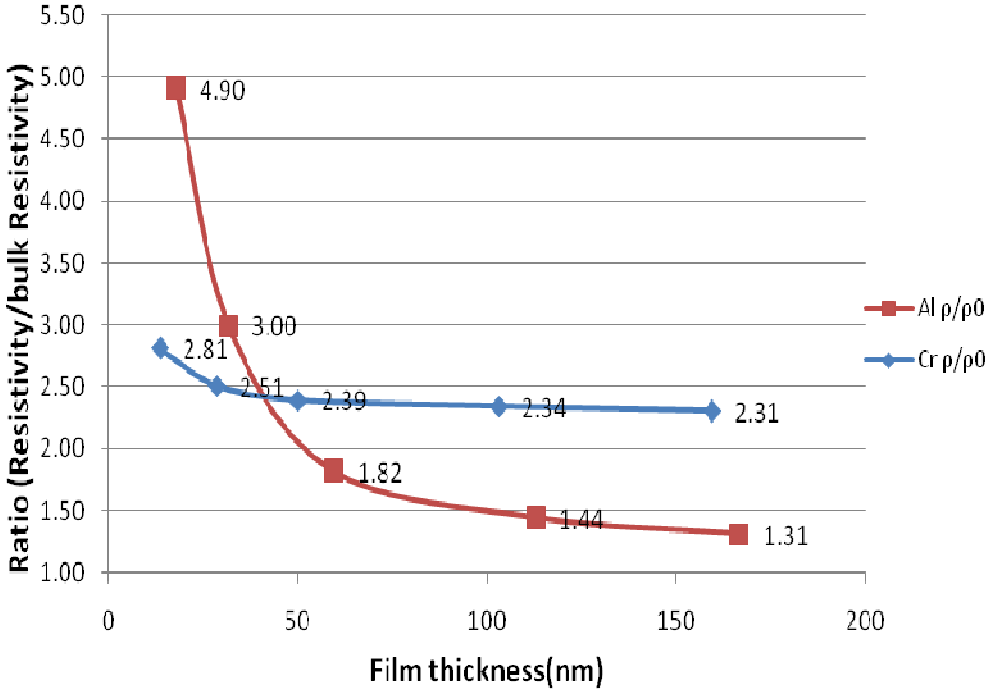

Figure 4.12 The aluminum and chromium resistivity ratios as a function of film thickness

Currently copper is the dominant material used for interconnects, replacing aluminum several years ago due to its lower resistivity [34]. Lower resistivity increases the energy efficiency. However, as new techniques develop for the next generations of microelectronic devices and transistors, the scale of everything becomes smaller. Predicted by Gordon Moore in 1965 [35], Moore's Law states that with each new generation of integrated circuit the number of transistors would double. The scale for metal thin films and wires has reached the point the size effects become important. This will be more important as the scale decreases further. Unfortunately, the resistivity of copper thin films changes rapidly as the thickness decreases to less than 100 nm as shown earlier in figure 2.6. The copper resistivity data in this figure came from films deposited by ion beam deposition. Our films are grown by magnetron sputtering. Although the deposition methods are different, a rough comparison of figure 2.6 and 4.11 shows that the differences in resistivity of the two metal films are much smaller when the thickness is lower than 50nm.

The scaling trend of resistivity appears to vary from metal to metal, this means that in the nano region, copper may not have the lowest resistivity. This may open up unique opportunities to new metal applications in nanotechnology.

Figure 4.13 shows several SEM images at 50,000x magnification of sputtered aluminum films of different thickness. The pictures show that

with increased film thickness, the patterns of the film surfaces were similar but the size of the crystallites increased.

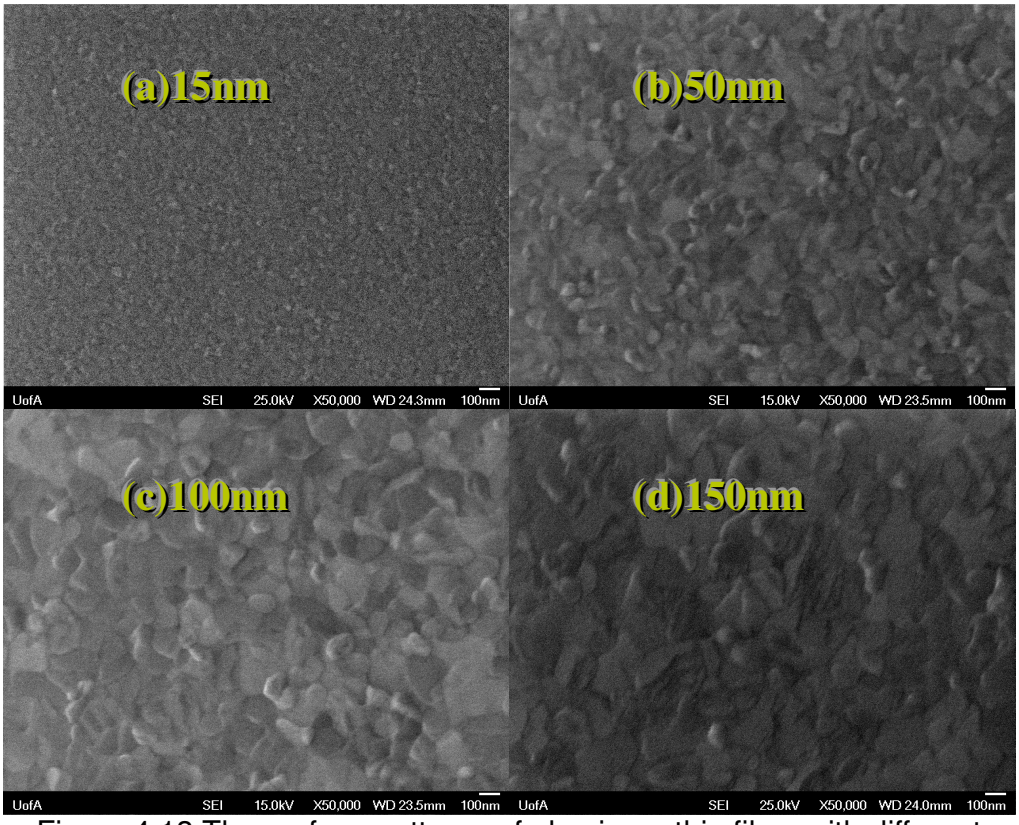

Figure 4.13 The surface patterns of aluminum thin films with different thickness captured by SEM (a) 15 nm (b) 50 nm (c) 100 nm (d) 150 nm

As discussed earlier, grain boundary scattering is one of the major factors that influence the resistivity of thin films. The average grain size of the thin film is a key factor that influences the film resistivity due to the MS theory [27]. Smaller grain size means more grain boundary per unit volume of the material and the size is approaching the mean free path of the electrons. The thin film surface and grain boundaries can act as additional scattering

centers for the electrons and causing collisions with the electrons. These collisions which affect the movement of electrons would influence the resistivity of the metal thin film. The grain size variation can be the reason of the size effect of the resistivity.

Due to current equipment limitations, annealing experiments and subsequent grain size measurement of metal thin film could not be done. However, the SEM images allow for possible grain size calculation and potential future work on finding and fitting the resistivity data to proper size effect models.

CHAPTER 5: CONCLUSIONS AND FUTURE WORK

5.1 Conclusions

The resistivity of sputtered metallic thin films showed that to choose an optimal argon working pressure is very important to gain a better film quality. The resistivity of titanium, chromium, copper, niobium and zirconium thin films (around 150 nm thick, sputtered at room temperature) had clearly increased as the sputtering argon pressure increased from 2 to 7 mTorr or 9 mTorr. The Zone Model of metal coating did explain the observed behavior well. These metal thin films had a structure change as the argon pressure increased. The steady resistivity of aluminum and tantalum as a function of argon pressure also fit the Zone Model due to their melting points and T/T_m ratio. Each of these two metals stays in one kind of Zone structure within the testing argon pressure range.

Further investigation on chromium thin films provided further evidence of Zone structure and structure change with the variation of argon pressure. X-ray tests showed a polycrystalline structure of chromium sputtered films 150 nm thick. The SEM images provided visual evidence of Zone 1 to Zone T in the changing surface microstructure of chromium thin films sputtered under different argon pressures. XPS results presented evidence of the porous structure of 7 mTorr sputtered chromium film and

the relatively compact and dense structure of 1 mTorr sputtered film in terms of surface composition and surface oxidation.

The comparison of thin film resistivity on different sputtering systems showed that base pressure and cleanliness of the chamber are also important issues affecting the film quality. Sputtering systems with lower base pressure and a load lock system produced metallic thin films with superior electrical properties.

The resistivity of aluminum and chromium sputtered thin films increased as the thickness of the film decreased from 100 nm to 15 nm. As well, the increased resistivity of aluminum was more than that of chromium as the film thickness decreased. The reason for resistivity increases at sub 100 nm film thickness is due to the size effect. It is due to higher contributions of surface scattering and grain boundary scattering to the total resistivity for lower film thickness. SEM images showed decreased grain sizes at the surface of aluminum thin films with decreased thickness.

5.1 Future work

A natural extension of this thesis work would be to investigate optimal argon pressure for more metals to acquire better film resistivity. Determining critical argon pressures for different metals would be useful. Due to Zone Model, temperature is another important factor that affects the microstructure of sputtered metal thin films. Its influences would be

very interesting and useful to determine. Other properties of metal films like mechanical properties could also be considered for determining optimal argon pressure in specific applications.

This work is an initial investigation on the size effect in sputtered metal thin films. Extensions of this work would require other equipment. Comparison of copper thin films and aluminum thin films with sub 100 nm thickness would be interesting and possibly useful. The size effect of other metals should also be investigated. Possible alternate materials to copper interconnections could be examined. With annealing experiments and grain size measurement experiments, proper models of the size effect of the sputtered metal thin films, combining FS theory and MS theory, could be developed.

REFERENCES

[1] Shyam P. Murarka, *Metallization: Theory and Practice for VLSI and ULSI*, Butterworth-Heinemann Pub. 1993

[2] John. Vossen, Werner Kern, *Thin Film Processes*, Academic Press, New York, 1978.

[3] Pawan Kapur, James P. McVittie, "Technology and Reliability Constrained Future Copper Interconnects — Part I: Resistance Modeling", IEEE TRANSACTIONS ON ELECTRON DEVICES, Vol. 49, No. 4, pp. 590-597, 2002

[4] K. Wasa, M. Kitabatake and H. Adachi, *Thin Film Material Technology: Sputtering of Compound Materials*, William Andrew Pub., New York, 2004.

[5] Rointan F. Bunshah, *Handbook of Hard Coatings: Deposition Technologies, Properties and Applications*, William Andrew Pub., New York, 2001

[6] Nils Laegreid, G. K. Wehner, "Sputtering yields of metals for Ar^+ and Ne^+ Ions with Energies from 50 to 600 eV", J. Appl. Phys. Vol. 32, No. 3, pp. 365-369, 1961.

[7] Raul A. Baragiola, "Sputtering: survey of observations and derived principles", Philosophical Transactions of the Royal Society A, Vol.362, No. 1814, PP. 29-53, 2004

[8] P. J. Kelly, R. D. Arnell, "Magnetron sputtering: a review of recent

developments and applications", Vacuum, Vol. 56, pp. 159-172, 2000.

[9] Rointan F. Bunshah, et al., *Deposition Technologies for Films and Coatings: Developments and Applications*, Noyes Pub., 1982.

[10] Seshan, Krishna, *Handbook of Thin-Film Deposition Processes and Techniques - Principles, Methods, Equipment and Applications (2nd Edition)*, William Andrew Pub., New York, 2002

[11] Donald L. Smith, *Thin-film Deposition: Principles and Practice*, McGraw-Hill, New York, 1995.

[12] Robert H. Havemann, “High-Performance Interconnects: An Integration Overview”, Proceedings of the IEEE, Vol. 89, No. 5, pp. 586-601, 2001.

[13] Pawan Kapur, James P. McVittie, "Technology and Reliability Constrained Future Copper Interconnects — Part II: Performance Implications", IEEE TRANSACTIONS ON ELECTRON DEVICES, Vol. 49, No. 4, pp. 598-604, 2002

[14] D. W. Hoffman, John A. Thornton, "Internal stresses in sputtered chromium", Thin Solid Films, Vol. 40, pp. 355-363, 1977.

[15] John A. Thornton, David W. Hoffman, "Internal stresses in titanium, nickel, molybdenum, and tantalum films deposited by cylindrical magnetron sputtering", J. Vac. Sci. Technol., Vol.14, No. 1, pp164-168, 1977.

[16] D. W. Hoffman, John A. Thornton, "The compressive stress transition in Al, V, Zr, Nb and W metal films sputtered at low working pressure", Thin

Solid Films, Vol. 45, pp. 387-396, 1977.

[17] John A. Thornton, "Influence of apparatus geometry and deposition conditions on the structure and topography of thick sputtered coatings", J. Vac. Sci. Technol., Vol. 11, No. 4, pp. 666-670, 1974.

[18] John A. Thornton, "Influence of substrate temperature and deposition rate on structure of thick sputtered Cu coatings", J. Vac. Sci. Technol., Vol. 12, No. 4, pp. 830-835, 1975.

[19] John A. Thornton, "High rate thick film growth", Ann. Rev. Mater. Sci., Vol.7, pp. 239-260, 1977.

[20] R. Messier, A. P. Giri, R. A. Roy, "Revised structure zone model for thin film physical structure", J. Vac. Sci. Technol., Vol. 2, No. 2, pp. 500-503, 1984

[21] P. Barna, M. Adamik, "Fundamental structure forming phenomena of polycrystalline films and the structure zone models", Thin Solid Films, Vol. 317, pp. 27-33, 1998

[22] K. Ellmer, "Magnetron sputtering of transparent conductive zinc oxide: relation between the sputtering parameters and the electronic properties", J. Phys. D-Appl. Phys., Vol.33, pp. R17-R32, 2000

[23] J. W. Lim, K. Mimura, M. Isshiki, "Thickness dependence of resistivity for Cu films deposited by ion beam deposition", Applied Surface Science, Vol. 217, pp. 95-99, 2003.

[24] S. M. Rossnagel, T. S. Kuan, "Alteration of Cu conductivity in the size effect regime", J. Vac. Sci. Technol. B, Vol. 22, No. 1, pp. 240-247, 2004

[25] K. Fuchs, "The conductivity of thin metallic films according to the electron theory of metals", Cambridge Philos. Soc., pp.100-108, 1938.

[26] E. H. Sondheimer, "The influence of a transverse magnetic field on the conductivity of thin metallic films", Physical Review, Vol. 80, No. 3, pp. 401-406, 1950.

[27] A. F. Mayadas, M. Shatzkes, "Electrical-resistivity model for polycrystalline films: the case of arbitrary reflection at external surfaces", Physical Review B, Vol. 1, No. 4, 1970.

[28] Niraj Joshi, A. K. Debnath, D. K. Aswal, et al., "Morphology and resistivity of Al thin films grown on Si (111) by molecular beam epitaxy", Vacuum, Vol. 79, pp. 178-185, 2005.

[29] H. Marom, M. Ritterband, M. Eizenberg, "The contribution of grain boundary scattering versus surface scattering to the resistivity of thin polycrystalline films", Thin Solid Films, Vol.510, pp. 62-67, 2006.

[30] Tik Sun, Bo Yao, Andrew P. Warren, et, al. "Dominant role of grain boundary scattering in the resistivity of nanometric Cu films", Physical Review B, Vol. 79, 041402, 2009.

[31] M. Cattani, A. R. Vaz, et, al., "Influence of electron scattering from morphological granularity and surface roughness on thin film electrical resistivity", Surface Review and Letters, Vol.14, No. 1, pp. 87-91, 2007.

[32] Equipment manual, Nanofab, University of Alberta.

[33] The Periodic Table of Elements

http://www.corrosionsource.com/handbook/periodic/

[35] Moore's Law

http://www.intel.com/cd/corporate/techtrends/emea/eng/209729.htm

APPENDIX

Table A1 Sputtering data of aluminum thin films sputtered with BOB

Al, Atomic Number 13, Melting Point 660℃

P (mTorr)	2	4	6	7	Pressure
Rs (Ω/m^2)	0.462	0.498	0.525	0.562	Average sheet resistance
t (nm)	134	120.25	118.38	109.38	Average thickness
ρ (Ω·m)	6.192E-08	5.992E-08	6.221E-08	6.144E-08	Resistivity
ρ_0 (Ω·m)	2.650E-08	2.650E-08	2.650E-08	2.650E-08	Bulk resistivity
ρ/ρ_0	2.34	2.26	2.35	2.32	Ratio
Time (min)	15	15	18	18	Deposition time
Rate (nm/min)	8.933	8.017	6.577	6.077	Deposition rate

Table A2 Sputtering data of titanium thin films sputtered with BOB

Ti, Atomic Number 22, Melting Point 1668℃

P (mTorr)	2	4	6	7	Pressure
Rs (Ω/m^2)	14.115	10.152	16.969	27.873	Average sheet resistance
t (nm)	122.5	170	149	110	Average thickness
ρ (Ω·m)	1.729E-06	1.726E-06	2.528E-06	3.066E-06	Resistivity
ρ_0 (Ω·m)	4.200E-07	4.200E-07	4.200E-07	4.200E-07	Bulk resistivity
ρ/ρ_0	4.12	4.11	6.02	7.30	Ratio

Table A3 Sputtering data of chromium thin films sputtered with BOB

Cr Atomic Number 24, Melting Point 1875℃

P (mTorr)	2	4	6	7	Pressure
Rs (Ω/m^2)	5.037	6.981	13.681	15.638	Average sheet resistance
t (nm)	155	136.5	172.5	155.75	Average thickness
ρ (Ω·m)	7.808E-07	9.529E-07	2.360E-06	2.436E-06	Resistivity
ρ_0 (Ω·m)	1.250E-07	1.250E-07	1.250E-07	1.250E-07	Bulk resistivity
ρ/ρ_0	6.25	7.62	18.88	19.48	Ratio

Table A4 Sputtering data of copper thin films sputtered with BOB

Cu Atomic Number 29, Melting Point 1085℃

P (mTorr)	2	4	6	7	Pressure
Rs (Ω/m^2)	0.145	0.217	0.308	0.208	Average sheet resistance
t (nm)	190.9	202.6	200.7	288.5	Average thickness
ρ (Ω·m)	2.767E-08	4.405E-08	6.182E-08	6.012E-08	Resistivity
ρ_0 (Ω·m)	1.680E-08	1.680E-08	1.680E-08	1.680E-08	Bulk resistivity
ρ/ρ_0	1.65	2.62	3.68	3.58	Ratio

Table A5 Sputtering data of zirconium thin films sputtered with BOB

Zr Atomic Number 40, Melting Point 1852℃

P (mTorr)	2	4	6	7	9	Pressure
Rs (Ω/m^2)	7.157	7.139	7.687	8.100	14.451	Average sheet resistance
t (nm)	162.17	168.75	169.67	180	179.13	Average thickness
ρ (Ω·m)	1.16E-06	1.21E-06	1.30E-06	1.46E-06	2.59E-06	Resistivity
ρ_0 (Ω·m)	4.24E-07	4.24E-07	4.24E-07	4.24E-07	4.24E-07	Bulk resistivity
ρ/ρ_0	2.74	2.84	3.08	3.44	6.11	Ratio
Time (min)	16	16	15	16	15	Deposition time
Rate (nm/min)	10.136	10.547	11.311	11.250	11.942	Deposition rate

Table A6 Sputtering data of niobium thin films sputtered with BOB

Nb Atomic Number 41, Melting Point 2468℃

P (mTorr)	2	4	6	7	Pressure
Rs (Ω/m^2)	7.955	4.485	7.973	18.347	Average sheet resistance
t (nm)	125	156.67	175	143.33	Average thickness
ρ (Ω·m)	9.943E-07	7.026E-07	1.395E-06	2.630E-06	Resistivity
ρ_0 (Ω·m)	1.520E-07	1.520E-07	1.520E-07	1.520E-07	Bulk resistivity
ρ/ρ_0	6.54	4.62	9.18	17.30	Ratio

Table A7 Sputtering data of tantalum thin films sputtered with BOB

Ta Atomic Number 73, Melting Point 3017℃

P (mTorr)	2	4	6	7	9	Pressure
Rs (Ω/m^2)	13.685	11.769	11.447	15.955	11.783	Average sheet resistance
t (nm)	136.83	155	158.83	122	170.75	Average thickness
ρ (Ω·m)	1.87E-06	1.82E-06	1.82E-06	1.95E-06	2.01E-06	Resistivity
ρ_0(Ω·m)	1.35E-07	1.35E-07	1.35E-07	1.35E-07	1.35E-07	Bulk resistivity
ρ/ρ_0	13.87	13.51	13.47	14.42	14.90	Ratio

Table A8 Sputtering data of aluminum thin film sputtered with Floyd

Predict Thickness(nm)	15	30	50	100	150	
Rs(Ω/m2)	7.320	2.501	0.811	0.338	0.208	Average sheet resistance
t(nm)	17.75	31.75	59.5	113	167	Average thickness
ρ(Ω·m)	1.30E-07	7.94E-08	4.83E-08	3.82E-08	3.48E-08	Resistivity
ρ_0(Ω·m)	2.65E-08	2.65E-08	2.65E-08	2.65E-08	2.65E-08	Bulk resistivity
ρ/ρ_0	4.90	3.00	1.82	1.44	1.31	Ratio

Table A9 Sputtering data of chromium thin film sputtered with Floyd

Predict Thickness(nm)	15	30	50	100	150	
Rs(Ω/m2)	26.025	11.003	5.984	2.845	1.807	Average sheet resistance
t(nm)	13.5	28.5	50	103	159.5	Average thickness
ρ(Ω·m)	3.51E-07	3.14E-07	2.99E-07	2.93E-07	2.88E-07	Resistivity
ρ_0(Ω·m)	1.25E-07	1.25E-07	1.25E-07	1.25E-07	1.25E-07	Bulk resistivity
ρ/ρ_0	2.81	2.51	2.39	2.34	2.31	Ratio